Ocean Sci., 3, 461–482, 2007
www.ocean-sci.net/3/461/2007/

Ocean Science

Effects of mesoscale eddies on global ocean distributions of CFC-11, CO_2, and $\Delta^{14}C$

Z. Lachkar[1,*], J. C. Orr[2], J.-C. Dutay[1], and P. Delecluse[1,]**

[1]LSCE/IPSL, Laboratoire des Sciences du Climat et de l'Environnement, CEA-CNRS-UVSQ, Gif-sur-Yvette, France
[2]Marine Environment Laboratories, International Atomic Energy Agency, Monaco
[*]now at: Institute of Biogeochemistry and Pollutant Dynamics, ETH Zurich, Zurich, Switzerland
[**]now at: Centre National de Recherches Météorologiques, Meteo-France, Paris, France

Received: 19 June 2006 – Published in Ocean Sci. Discuss.: 31 July 2006
Revised: 17 July 2007 – Accepted: 4 October 2007 – Published: 12 October 2007

Abstract. Global-scale tracer simulations are typically made at coarse resolution without explicitly modelling eddies. Here we ask what role do eddies play in ocean uptake, storage, and meridional transport of transient tracers. We made global anthropogenic transient-tracer simulations in coarse-resolution ($2° \cos\varphi \times 2°$, ORCA2) and eddy-permitting ($\frac{1}{2}° \cos\varphi \times \frac{1}{2}°$, ORCA05) versions of the ocean general circulation model OPA9. Our focus is on surface-to-intermediate waters of the southern extratropics where air-sea tracer fluxes, tracer storage, and meridional tracer transport are largest. Eddies have little effect on global and regional bomb $\Delta^{14}C$ uptake and storage. Yet for anthropogenic CO_2 and CFC-11, refining the horizontal resolution reduced southern extratropical uptake by 25% and 28%, respectively. There is a similar decrease in corresponding inventories, which yields better agreement with observations. With higher resolution, eddies strengthen upper ocean vertical stratification and reduce excessive ventilation of intermediate waters by 20% between 60° S and 40° S. By weakening the residual circulation, i.e., the sum of Eulerian mean flow and the opposed eddy-induced flow, eddies reduce the supply of tracer-impoverished deep waters to the surface near the Antarctic divergence, thus reducing the air-sea tracer flux. Thus in the eddy permitting model, surface waters in that region have more time to equilibrate with the atmosphere before they are transported northward and subducted. As a result, the eddy permitting model's inventories of CFC-11 and anthropogenic CO_2 are lower in that region because mixed-layer concentrations of both tracers equilibrate with the atmosphere on relatively short time scales (15 days and 6 months, respectively); conversely, bomb $\Delta^{14}C$'s air-sea equilibration time of 6 years is so slow that, even in the eddy permitting model, there is little time for surface concentrations to equilibrate with the atmosphere, i.e., before surface waters are subducted.

Correspondence to: Z. Lachkar
(zouhair.lachkar@env.ethz.ch)

1 Introduction

The ocean's large capacity to take up and store carbon mediates the increase of anthropogenic CO_2 in the atmosphere. Thus, accurately determining ocean uptake of anthropogenic tracers is relevant not only to understanding the global carbon cycle, but also to predicting the magnitude of future climate change. Ocean models have been used extensively to understand air-sea fluxes and ocean storage of anthropogenic carbon. Storage of anthropogenic carbon has also been estimated with data-based approaches (Gruber et al., 1996; Sabine et al., 2004), but these are not without substantial random and systematic errors (Matsumoto and Gruber, 2005).

During the last decade, the Ocean Carbon-Cycle Model Intercomparison Project (OCMIP) examined and compared several existing ocean general circulation model (OGCM) simulations of transient tracers (Orr et al., 2001; Dutay et al., 2002; Watson and Orr, 2003; Matsumoto et al., 2004). All the OCMIP models used a coarse-horizontal grid and resorted to parameterising the effect of unresolved subgrid mixing processes on larger scales. The OCMIP models disagree substantially in terms of the simulated anthropogenic CO_2 air-sea flux within the southern extratropics (the region south of 20° S), which absorbs up to half of the global oceanic uptake (Orr et al., 2001; Watson and Orr, 2003). More recently, Matsumoto et al. (2004) compared simulated natural radiocarbon, anthropogenic CO_2, and CFC-11 from 19 ocean carbon cycle models with data-based estimates and also found large discrepancies between model results. These model discrepancies are partly associated with differences in the representation of subgrid-scale ocean mixing processes

Published by Copernicus Publications on behalf of the European Geosciences Union.

(Matear, 2001; Dutay et al., 2002). In the only attempt to date to use a global eddy resolving model (1/10°) to simulate the ocean CFC-11 distribution, Sasai et al. (2004) demonstrated much improved agreement with the observations in the southern extratropics. In particular, their model exhibits improved skill south of 40° S with none of the excessive ventilation of thermocline and intermediate waters that is characteristic of most of the OCMIP coarse-resolution models. Thus, generally improving the ability to account for mesoscale eddies may be key to correctly simulating the uptake, transport, and storage of the transient tracers, especially in southern extratropics. To improve eddy parameterisations for coarse-resolution models, ocean modellers can learn from how ocean eddies affect global and regional ocean tracer budgets.

During the past three decades, physical oceanographers have made significant advances in discerning the role that eddies play in the ocean's general circulation (Holland and Lin, 1975a,b; Holland, 1978). Cox (1985) investigated the effects of mesoscale eddies within the subtropical thermocline and highlighted the eddy-induced homogenisation of anomalous Potential Vorticity along isopycnals. In terms of meridional heat transport, Böning and Budich (1992) found a negligible effect of eddies when using a primitive equation model for an idealised ocean basin. Drijfhout (1994) showed that the eddy-induced mean meridional circulation nearly compensates poleward eddy heat transport for the case of a weak diabatic forcing. Vallis (2000) demonstrated how mesoscale eddies could be important in determining ocean stratification. Marshall et al. (2002) and Marshall and Radko (2003) used idealised simulations for a channel-only domain, finding that eddies help to set both the stratification and the depth of the permanent thermocline in the ocean.

Despite these advances, all studies have been limited by the compromises that must be made because of the computer-intensive nature of making simulations that include mesoscale variability in global-scale numerical models. Previous work has generally used simplified basin-scale models to investigate the genesis of mesoscale eddies and their interaction with the mean flow. Few studies indeed have addressed how ocean eddies may affect global-scale transport and distribution of transient tracers. Here we attempt to elucidate the importance of mesoscale eddies in terms of their effect on the global distributions of transient tracers. To isolate the effect of eddies, we follow the lead of Cox (1985) and Thompson et al. (1997), who compared integrations of a noneddying and an eddying versions of the same model. Thus we also compare a coarse-resolution to an eddy-permitting version of the same OGCM.

In addition to anthropogenic CO_2, we also made simulations of CFC-11 and bomb $\Delta^{14}C$ to better evaluate model performance and to investigate how mesoscale eddies affect transient tracers with different air-sea equilibration times. That is, these three tracers require different times for their mixed-layer concentrations to equilibrate with the atmosphere. For a purely inert tracer, the equilibration time τ_{eq} can be estimated following Broecker and Peng (1974) as $\tau_{eq}=\frac{h}{v}$ where h is the mixed-layer depth and v the tracer piston velocity. Between 60° S and 40° S, the air-sea equilibration time for typical gaseous tracers, including CFC-11, is ∼14 days, whereas for bomb $\Delta^{14}C$ it is ∼6 years. Lying between these two extremes is the anthropogenic CO_2's air-sea equilibration time of ∼6 months. Equilibration for CO_2 is slower than for CFC-11 because when added to seawater, CO_2 does not remain a dissolved gas as does CFC-11; instead, it reacts with carbonate ion CO_3^{2-} to form bicarbonate ion HCO_3^-. What matters then is the change in the mixed-layer concentration of the sum of these three species (i.e., dissolved inorganic carbon DIC), not just the change in CO_2 concentration. Relative to CFC-11, the time for a perturbation in mixed-layer DIC to equilibrate with the atmosphere is longer by a factor of $\frac{\partial[DIC]}{\partial[CO_2*]}$ (Sarmiento and Gruber, 2006). That factor averages 12 between 60° S and 40° S whereas it averages 19 globally, based on the GLODAP data. For bomb $\Delta^{14}C$, the equilibration time between the mixed layer and the atmosphere is much longer still because isotopic equilibrium requires that CO_2 exchange its isotopic composition with the entire DIC pool. The corresponding factor is then $\frac{[DIC]}{[CO_2*]}$, which averages 140 between 60° S and 40° S and 180 globally.

The air-sea equilibration time has already been shown to affect transport and uptake of transient tracers in an idealised model of the Southern Ocean (Ito et al., 2004). Here we aim to use an OGCM to evaluate the effects of mesoscale eddies on large-scale uptake, storage, and meridional transport of CFC-11, anthropogenic CO_2, and bomb $\Delta^{14}C$, while focusing particularly on the southern extratropics where uptake and storage are largest. We also aim to investigate how mesoscale eddies alter ocean dynamics in the higher southern latitudes and to examine the mechanisms by which they affect large-scale distributions of transient tracers.

2 Methods

2.1 Strategy

We made a series of simulations for CFC-11, anthropogenic CO_2 and bomb $\Delta^{14}C$, using a noneddying version of the model having a $2° \cos\varphi \times 2°$ coarse-grid (termed ORCA2), where φ is latitude. We also made analogous simulations with an eddying version of the same model using a $\frac{1}{2}° \cos\varphi \times \frac{1}{2}°$ grid (ORCA05), whose grid size is 34 km on average, globally, and is 28 km at 60° S. The eddying version of the model has sufficient horizontal resolution to resolve the largest mesoscale eddies (those with diameter larger than two or three times the grid size), although it does not resolve the rest of the mesoscale eddy spectrum. For comparison, to be fully "eddy-resolving" there would need to be at least 12 grid points per wavelength (Chassignet and Verron, 2006),

i.e., a grid size at least six times smaller than the first Rossby Radius of deformation, which varies between 10 and 20 km in high latitudes (Chelton et al., 1998). The main goal of this work is to explore how simulated ocean uptake of transient tracers changes as one begins to explicitly resolve mesoscale eddies, i.e., when moving from a coarse-resolution to an eddy-permitting OGCM. We will address if crossing that threshold is important in terms of transient tracer uptake, although studying the effects of moving to finer resolution is beyond the scope of this study.

Although the eddying model does not resolve the entire spectrum of mesoscale eddies, it does exhibit substantial eddy activity in the Southern Ocean along some of the most energetic currents in the world (Fig. 1); conversely, the coarse-resolution model exhibits no such activity. In a first series of two simulations at eddying and noneddying resolution, we deliberately avoided using any subgrid-scale eddy parameterisation in order to better capture the effect of resolving mesoscale eddies that goes along with an increase in horizontal resolution. Additionally, in order to assess the effectiveness of the most widely used eddy parameterisation, known as GM (Gent and McWilliams, 1990; Gent et al., 1995), to represent the role of mesoscale eddies in ocean uptake of transient tracers, we made two other CFC-11 simulations using this parameterisation at both resolutions. The GM coefficients of thickness diffusivity and isopycnal diffusivity in both simulations were set to $10^3 m^2\ s^{-1}$.

Integrating long global carbon simulations until near-steady state requires running the model for several thousand years. At eddy-permitting resolution, that would extend far beyond presently available computing resources. To overcome this technical limitation, we used perturbation approaches for both anthropogenic CO_2 and bomb $\Delta^{14}C$. In so doing, we assume that the natural ocean carbon cycle is not affected directly by the anthropogenic perturbation. Thus we treat anthropogenic CO_2 and bomb $\Delta^{14}C$ as passive tracers excluding any possible response of the ocean biological process to the anthropogenic CO_2 increase. This approach was introduced for anthropogenic CO_2 by Siegenthaler and Joos (1992) and first used in a 3-D model by Sarmiento et al. (1992). Here we extend it to bomb $\Delta^{14}C$. Simulations of anthropogenic CO_2 begin on 1 January 1765 and are run until 1 January 2000 (industrial era); simulations for bomb $\Delta^{14}C$ start on 1 July 1954 and run until 1 January 2000 (nuclear era).

Despite the advantage of using a perturbation approach, realising online global tracer simulations in an eddying, global-scale OGCM remains a challenge because of the computational requirements. For example, a 235-year anthropogenic CO_2 simulation (1765–2000) with our eddying model requires 11 000 CPU-hours on one processor of a NEC-SX6 vectorial supercomputer. To further reduce computational costs we used the offline approach for our tracer simulations. An offline model driven by monthly fields from an (online) eddy-permitting OGCM ($0.4° \cos\varphi \times 0.4°$) was

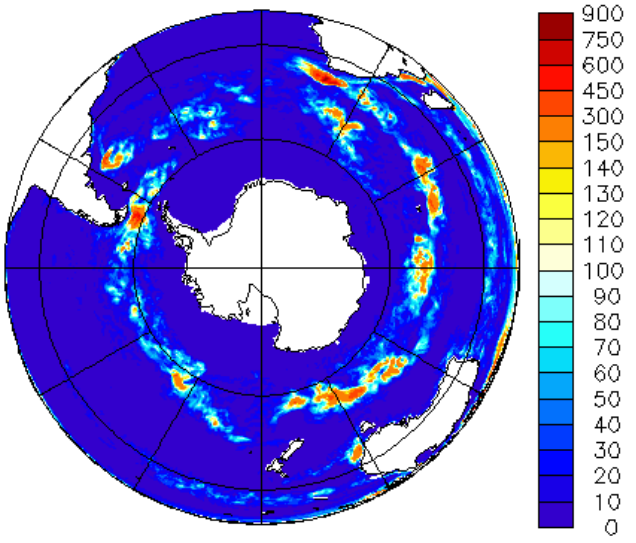

Fig. 1. Surface-ocean eddy kinetic energy in the southern extratropics (in $cm^2\ s^{-2}$) of the eddying simulation.

used by Sen Gupta and England (2004) to investigate ventilation of globally prominent water masses. Hill et al. (2004) used a 1/6° North Atlantic regional model, finding that offline simulations remain faithful to online runs when the time-averaged flow fields are updated on a timescale close to the inertial period (about 1 day). Here, small eddies associated with high frequency time variability (close to the inertial period) are not present in the flow given that we resolve only the upper range of mesoscale spectrum. Thus we used a 5-day forcing frequency for both eddying and noneddying simulations. With the noneddying version of our model, the offline transient-tracer results closely resemble those obtained with the online version, e.g., with zonal means of the inventory differing at most by 3%.

To evaluate simulations, we compared simulated to observed tracer distributions along vertical sections from the World Ocean Circulation Experiment (WOCE) and to gridded data products from Global Ocean Data Analysis Project (GLODAP). The GLODAP data consists of synthesised products from WOCE, the Joint Global Ocean Flux Study (JGOFS), and the Ocean Atmosphere Carbon Exchange Study (OACES) (Key et al., 2004).

2.2 Models

Our simulations were made with the ORCA-LIM global coupled ocean-sea ice model whose ocean component is based on version 9 of the model OPA (Océan PArallélisé, referred to as OPA9). OPA is a finite difference OGCM with a free surface and a nonlinear equation of state following the Jackett and McDougall (1995) formulation (Madec and Imbard, 1996; Madec et al., 1998); The model has a contorted horizontal curvilinear mesh in order to overcome the North Pole

singularity found in conventional grids. To avoid the typical northern singularity over the ocean, the OPA9 grid has two poles, one over Canada and the other over Asia, which allows for longer timesteps while still respecting the CFL stability criterion. Variables are distributed on C grid (Arakawa, 1972) on prescribed z-levels. The horizontal grid is also orthogonal and retains numerical accuracy to the second order (Marti et al., 1992). The model is implemented on a Mercator grid, i.e., becoming finer at high latitudes following the cosine of latitude. With 46 levels in the vertical direction, the vertical grid spacing increases from 6 m at the surface to 250 m at the bottom. The bottom of the deepest level reaches 5750 m. Lateral tracer mixing occurs along isopycnal surfaces via Laplacian diffusion. For the noneddying model, we used horizontal Laplacian diffusion operator, as is typical for coarse-resolution models. For the eddying model, we used the biharmonic formulation for viscosity, in order to make optimal use of the resolved scales and to allow the eddying flow to exhibit its dominant nondiffusive nature (Griffies and Hallberg, 2000). The biharmonic diffusion operator has no advantage at coarse resolution but is much better suited for eddying models because it acts on smaller scales, admitting shorter wavelength structures on the mesh that would be damped out by the Laplacian operator (Griffies et al., 2000). Vertical eddy diffusivity and viscosity coefficients are given by a second-order closure scheme based on a prognostic equation for turbulent kinetic energy (TKE) (Gaspar et al., 1990; Blanke and Delecluse, 1993) and are enhanced in the case of static instability. This TKE parametrisation improves simulated equatorial dynamics and the thermocline in a high resolution model (Blanke and Delecluse, 1993). To advect temperature and salinity, we used the Total Variance Diminishing (TVD) advection scheme following Lévy et al. (2001).

The bathymetry is calculated using the 2′ bathymetry file ETOPO2 from NGDC (National Geophysical Data Center) (Smith and Sandwell, 1997; Jakobsson et al., 2000), except for the zone south of 72° S where it was computed from the BEDMAP data (Lythe and Vaughan, 2001). The OGCM output was stored as 5-day averages to avoid aliasing of high-frequency processes (Crosnier et al., 2001). Initial conditions for the temperature and salinity fields were taken from Levitus et al. (1998) for the low and middle latitudes and from the PHC2.1 climatology (Steele et al., 2001) for high latitudes.

The model was started from rest, then spun up for 8 years with a climatological seasonal forcing with daily frequency as computed from the 1992–2000 NCEP/NCAR 10-m wind stress and 2-m air temperature data (Kalnay et al., 1996). Additionally, we used monthly climatologies of precipitation (Xie and Arkin, 1996), relative humidity (Trenberth et al., 1989), and total cloud cover (Berliand and Strokina, 1980). Surface heat fluxes and freshwater flux for ocean and sea-ice were calculated using the empirical bulk parameterisation proposed by Goose (1997).

The sea ice component of ORCA-LIM is the Louvain-la-Neuve sea ice model (LIM), a dynamic-thermodynamic model specifically designed for climate studies. A full description of LIM is given by Fichefet and Maqueda (1997).

To study passive tracers, we used a tracer-transport (offline) version of OPA (OPA Tracer 8.5) driven by 5-day averages of fields of advection and vertical turbulent diffusion from the dynamic (online) model. As for active tracers (temperature and salinity), we used isopycnal Laplacian mixing with the same lateral diffusion coefficients as in the dynamic model. We employed the flux-corrected-transport advection scheme from Smolarkiewicz (1982, 1983); Smolarkiewicz and Clark (1986). This advection scheme is little diffusive and is positive definite, i.e., it ensures positive tracer concentrations.

2.3 Passive tracer boundary conditions

2.3.1 CFC-11

CFC-11 (chlorofluorocarbon-11) is a purely anthropogenic trace gas, whose atmospheric concentration has increased from zero since the 1930s. Once it enters the surface ocean via gas exchange, CFC-11 is chemically and biologically inert. Thus it serves as a passive conservative tracer and tracks circulation and mixing processes that occur over decadal timescales (Wallace and Lazier, 1988; Doney and Bullister, 1992; Waugh et al., 2003). The large database of oceanic concentrations of CFC-11 come from direct measurements made at ∼1% precision during the World Ocean Circulation Experiment (WOCE). Putting that high precision into context, the other two transient tracers can only be estimated indirectly from other data, which means errors are relatively much larger and unfortunately difficult to quantify (Matsumoto and Gruber, 2005; Key et al., 2004). To model CFC-11 ocean uptake, we followed the protocols defined by OCMIP-2 (Dutay et al., 2002). That is, passive tracer fluxes at the air-sea interface were calculated according to the classical formulation of air-sea gas exchange

$$F_{\mathrm{CFC}} = K_{\mathrm{CFC}}(p\mathrm{CFC} - \frac{C_s}{\alpha_{\mathrm{CFC}}})(1-I) \quad (1)$$

where K_{CFC} is the CFC-11 gas transfer coefficient (mol m^{-2} yr^{-1} µatm^{-1}), pCFC is the partial pressure of CFC-11 from the reconstructed atmospheric history (Walker et al., 2000), and C_s is the modelled sea surface tracer concentration. The α_{CFC} term is the CFC-11 solubility in the sea water (Warner and Weiss, 1985), which depends on temperature and salinity at the surface; I is the fractional sea ice cover, which varies between 0 and 1. K_{CFC} is calculated from solubility and 10-m NCEP wind speed using the Wanninkhof (1992) formulation of gas transfer velocity. Time and space variations of total air pressure are neglected.

2.3.2 Anthropogenic CO_2 Perturbation

For the anthropogenic CO_2 we used the same boundary conditions as developed for OCMIP-2. The air-sea CO_2 flux is

determined as:

$$F_{CO_2} = K_{CO_2}(\delta pCO_{2a} - \delta pCO_{2o})(1 - I) \quad (2)$$

where K_{CO_2} is the CO_2 gas transfer coefficient in $\mathrm{mol\,m^{-2}\,yr^{-1}\,ppm^{-1}}$ calculated following Wanninkhof (1992) and δpCO_{2a} and δpCO_{2o} are the atmospheric and the oceanic perturbations of carbon in ppm. The atmospheric perturbation is defined by

$$\delta pCO_{2a} = pCO_{2a} - pCO_{2a,0} \quad (3)$$

where pCO_{2a} is the partial pressure of atmospheric CO_2 as prescribed from the Enting et al. (1994) spline fit to Siple ice core and Mauna Loa atmospheric CO_2 data for 1765.0 to 1990.0 and from the 12-month smoothed GLOBALVIEW-CO_2 (2003) Mauna Loa data for 1990.5 to 2000.0. The $pCO_{2a,0}$ term is set to 278 ppm, the partial pressure of CO_2 at the beginning of simulation (1765).

Unlike CFC-11, CO_2 is highly soluble in seawater and is hydrolysed to form other inorganic carbon species, i.e., bicarbonate and carbonate ions. To model CO_2 then, we must carry the sum of all three dissolved inorganic species, i.e., DIC, and in the case of a perturbation approach, the model carries only the anthropogenic component (δDIC). Hence, at the surface, we need to convert between δDIC carried by the model and δpCO_{2o} that is needed to compute the air-sea flux according to Eq. (2).

To do so, we follow the lead of Siegenthaler and Joos (1992) and Sarmiento et al. (1992). That is, we express the oceanic perturbation in the partial pressure of CO_2 (pCO_{2o}) in terms of the perturbation in dissolved inorganic carbon (δDIC)

$$\delta pCO_{2o} = \frac{z_0[\delta\mathrm{DIC} + \delta\mathrm{DIC_{corr}}]}{1 - z_1[\delta\mathrm{DIC} + \delta\mathrm{DIC_{corr}}]} - pCO_{2a,\mathrm{corr}} \quad (4)$$

where z_0 and z_1 are coefficients that depend on temperature. Here though, we have added two correction factors, $\delta\mathrm{DIC_{corr}}$ and $pCO_{2a,\mathrm{corr}}$, to take into account that the starting value of $pCO_{2a,0}$ is different from the reference $pCO_{2a,\mathrm{ref}}$=280 ppm that Siegenthaler and Joos (1992) used when developing the perturbation approach. More details are offered in the appendix.

2.3.3 Bomb Δ^{14}C Perturbation

To model bomb Δ^{14}C, we treated the $^{14}C/^{12}C$ ratio as a concentration and used the perturbation approach. Therefore we do not simulate processes causing fractionation (Toggweiler et al., 1989a,b), which induces a small simulation error (Joos et al., 1997). As with any perturbation approach, the simulation must begin with the ocean and atmosphere containing zero bomb Δ^{14}C. Historical estimates of atmospheric $^{14}C/^{12}C$ are available for 3 latitudinal bands (90° S–20° S, 20° S–20° N, 20° N–90° N) from the compilation made for OCMIP-3 (I. Levin, personal communication; T. Naegler, personal communication). Our approach accounts for the anthropogenic perturbation in CO_2 atmospheric concentrations unlike Toggweiler et al. (1989b) who used the pre-industrial level for the atmospheric forcing. We force the 3-box atmosphere to maintain observed values of bomb Δ^{14}C that were shifted upward by subtracting off values from July 1954, which are negative due to the Suess effect. Bomb Δ^{14}C enters the ocean via air-sea exchange of CO_2. Radioactive decay is included but not important for the short simulations made here.

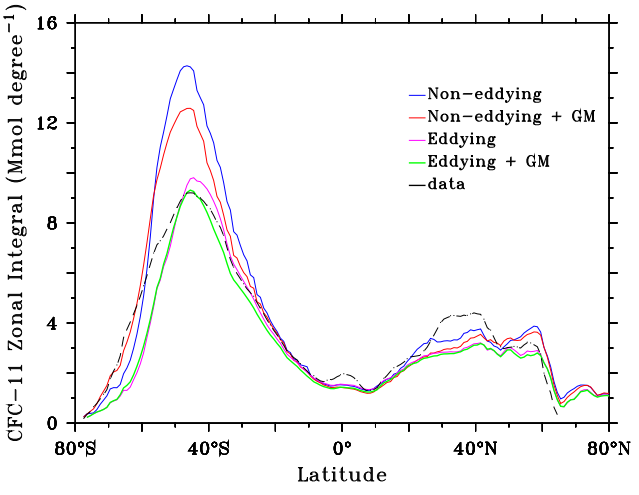

Fig. 2. Zonally integrated inventories of CFC-11 in 1994 as observed (black dashes, GLODAP) and as simulated by the noneddying model with GM (red) and without GM (blue) as well as by the eddying model with GM (green) and without GM (purple).

Following Orr et al. (2001), the air-sea bomb Δ^{14}C flux $F_{^{14}C}$ can be expressed as:

$$F_{^{14}\mathrm{C}} = \mu(C_a - C_o)(1 - I) \quad (5)$$

where C_a is atmospheric bomb Δ^{14}C ratio, C_o is the simulated surface ocean ratio, and the CO_2 replenishment rate μ is given by

$$\mu = K_{CO_2}\frac{pCO_{2a}}{\mathrm{DIC}} \quad (6)$$

where DIC is the surface ocean concentration of dissolved inorganic carbon (taken as $2.0\,\mathrm{mol\,m^{-3}}$) (Toggweiler et al., 1989a).

3 Results

3.1 Model evaluation

3.1.1 GM parameterisation

Simulations with and without the GM parameterisation reveal the extent to which the noneddying model with the GM

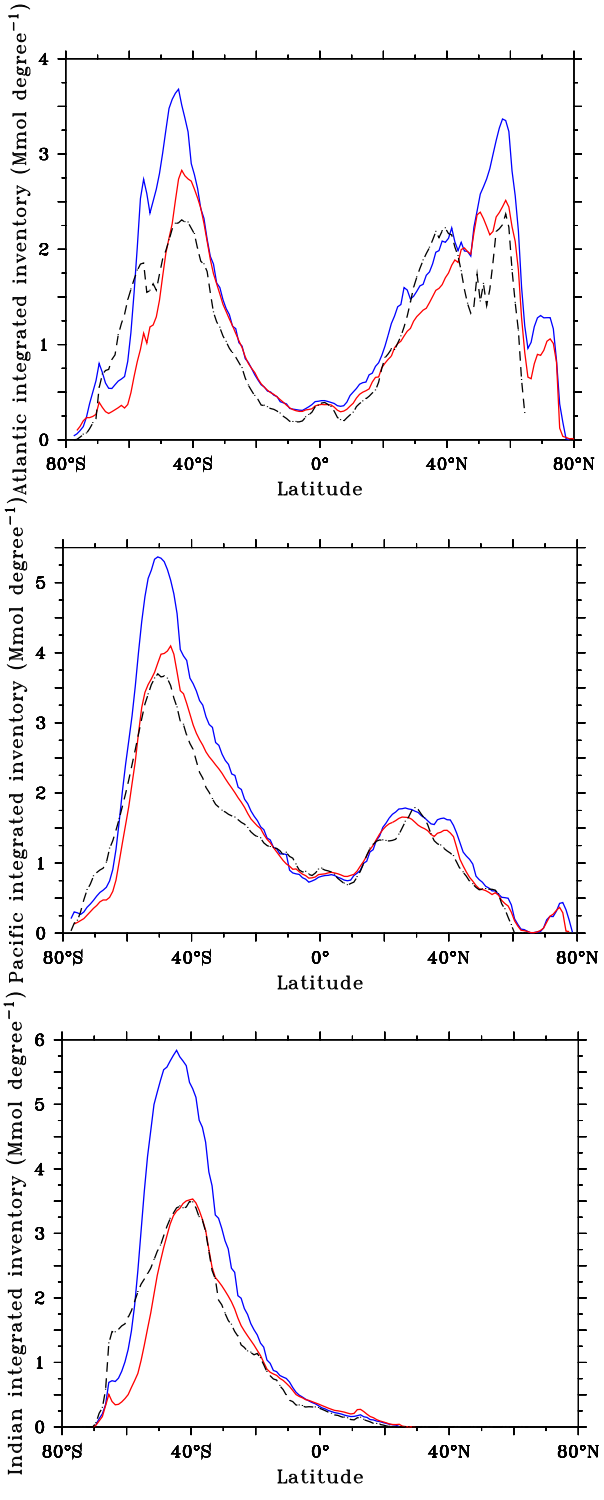

Fig. 3. Zonally integrated basin-scale inventories of CFC-11 for the Atlantic (upper), Pacific (middle), and Indian (lower) Oceans as observed (black dashes, GLODAP) and as simulated by the eddying (red) and noneddying (blue) models at end of year 1994.

parameterisation properly represents how CFC-11 is affected by mesoscale eddies in the eddying model. Figure 2 compares simulations of the eddying and noneddying models, both with and without GM, to the GLODAP global data product (Key et al., 2004) in terms of the vertical column integral of the CFC-11 concentration (inventory), integrated zonally across the globe. The eddying model matches the observed maximum in the CFC-11 inventory between 45° S and 50° S within 6%, whether or not it uses GM. In contrast, the noneddying model without GM overestimates this peak by 55%. Although the noneddying model with GM is better, it still overestimates the observed peak by 36% and remains far from the eddying model. This unrealistic result may be related to GM being an adiabatic parameterisation. There is an important diabatic component to eddy fluxes close to boundaries, particularly near the ocean surface (Robbins et al., 2000; Price, 2001). Thus GM misrepresents eddy diapycnal behaviour in the mixed layer and that may drive spurious exchange between the upper mixed layer and the ocean interior. But whatever the cause, our simple global analysis demonstrates that the GM parameterization in the noneddying model does not properly represent the role of mesoscale eddies in the eddying model. From here on then, we focus on the effect of resolution by comparing eddying and noneddying simulations without the GM parameterisation.

3.1.2 CFC-11

The global CFC-11 inventory in the noneddying model is 28% larger than that obtained by the eddying model, with the latter being closer to the observed estimates (Key et al., 2004; Willey et al., 2004) (see Table 3). Both gridded data products rely on the WOCE CFC-11 observations although they use different interpolation procedures. In addition, the global inventory of our eddying model is close to that of the global 1/10° eddy-resolving model of Sasai et al. (2004). As for meridional structure, Fig. 3 compares CFC-11 inventories from both models to the GLODAP data-based product (Key et al., 2004) over each of the three ocean basins. Higher resolution offers substantial improvement, particularly in the Indian basin where the coarse-resolution model overestimates the CFC-11 inventory by 64% between 50° S and 30° S. Conversely, south of 50°S near the Antarctic divergence, both model versions underestimate the observed inventory, mainly because the mixed layer is too shallow by 150 to 200 m (Fig. 4). This model deficiency in the upper ocean of the high southern latitudes is associated with insufficient vertical mixing produced by the current version of TKE scheme in OPA model. Additionally, formation of Antarctic Bottom Water (AABW) may be too weak. Yet despite this poor performance in the highest southern latitudes, there is little impact on basin-integrated inventories because discrepancies occur in a region that has relatively little surface area and tracer storage.

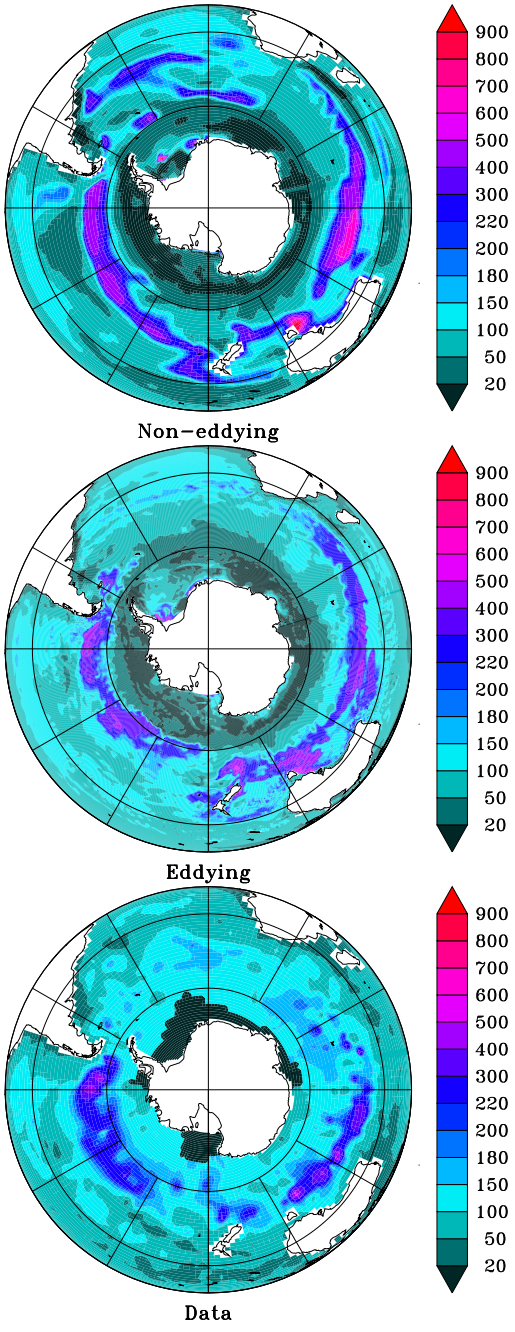

Fig. 4. Mixed-layer depth (m) in the southern extratropics in mid-September as simulated by the noneddying (top) and eddying (middle) models as well as that from an observational climatology (de Boyer Montégut et al., 2004) (bottom).

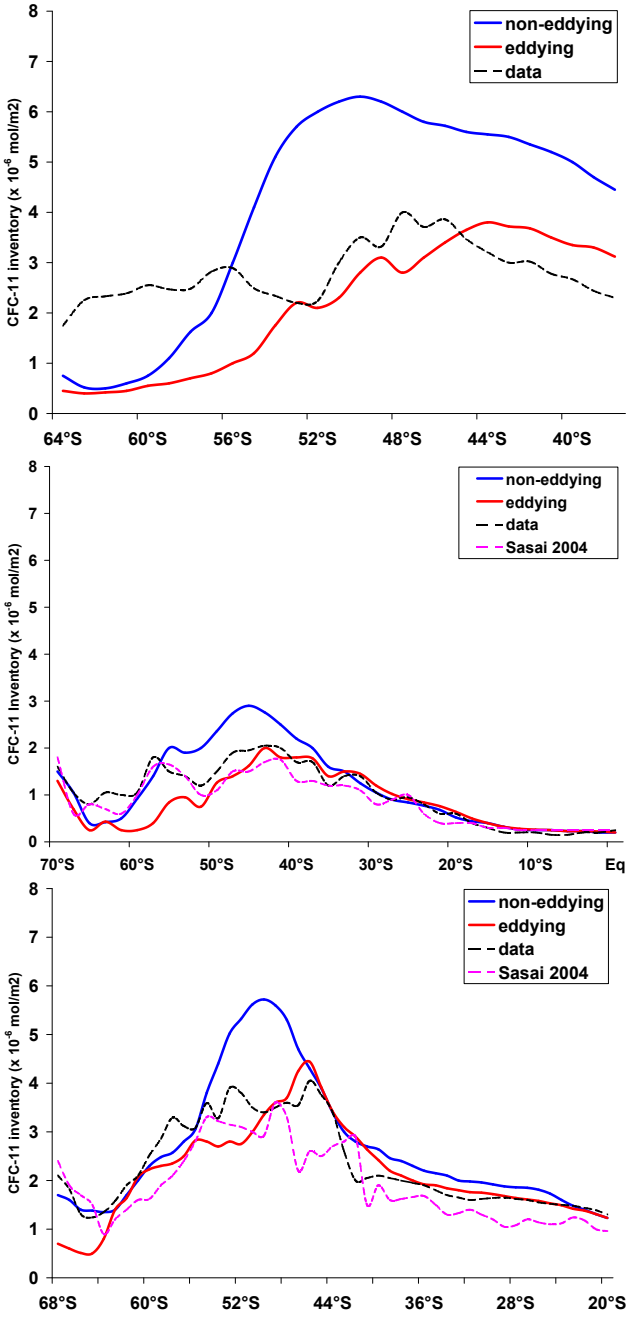

Fig. 5. CFC-11 inventories for the WOCE I9S section along 115° E in the Indian sector of the Southern Ocean (upper), the AJAX section along 0° E in the South Atlantic (middle), and the WOCE P15S section along 170° W in the South Pacific (lower), as observed (black) and as simulated by the noneddying (blue) and the eddying (red) models. The dashed purple curves show the Sasai et al. (2004) inventories.

Simulated CFC-11 column inventories were also compared to observations along three sections in the southern extratropics: AJAX along the Greenwich meridian in 1983 (Warner and Weiss, 1992), WOCE I9S along 115° E in the Indian Ocean (1994–1995), and WOCE P15 along 170° W in the South Pacific in 1996 (Fig. 5). Once again, increased resolution improves results north of 50° S in all three sections. The noneddying model overestimates observed CFC-11 inventories along all three sections, as do most of OCMIP

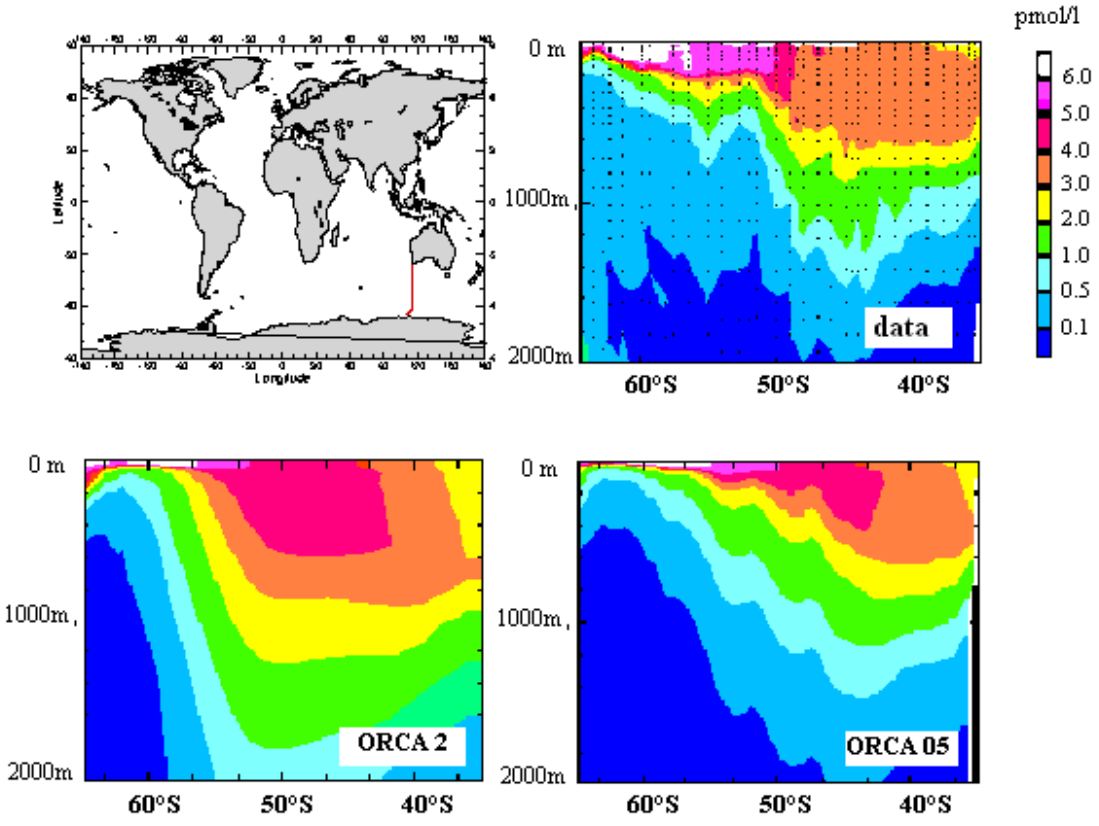

Fig. 6. CFC-11 concentration (in pmol l^{-1}) along the WOCE I9S section (115° E, 1994–1995) as observed and simulated by the noneddying (ORCA2) and the eddying (ORCA05) model.

coarse-resolution models that do not account for mesoscale processes (Dutay et al., 2002).

For greater detail south of 40° S, where the ocean storage is largest and where OCMIP models differ most (Dutay et al., 2002), we compared models to data along two deep sections: I9S in the Indian sector of the southern extratropics (Fig. 6) and AJAX in the South Atlantic (Fig. 7). As seen with Fig. 5, finer resolution leads to general improvement, particularly along the Indian section. Most notable is the eddying model's more realistic vertical penetration of CFC-11 north of Subantarctic Front (SAF), near 50° S. In the noneddying simulation, the vertical distribution is too diffusive which results in excessive penetration particularly in the Indian Ocean. South of 50° S, both model versions underestimate tracer penetration within the upper 200 m. We also compared modelled and observed CFC-11 in the North Atlantic on the Na20w meridional section, which runs mostly along 20° W (Fig. 8). Both the eddying and noneddying models reproduce the general features of the CFC-11 vertical penetration profile, but in the noneddying model, there appears to be too much ventilation where NADW forms between 55° N and 60° N. Overall, the eddying model is also more realistic along this North Atlantic meridional section.

3.1.3 Anthropogenic CO_2 and bomb $\Delta^{14}C$

Unlike for CFC-11, both the noneddying and eddying models simulate global anthropogenic CO_2 inventories that are within the uncertainty of GLODAP data-based estimate (Key et al., 2004; Sabine et al., 2004) (Table 3). For the global bomb $\Delta^{14}C$ inventory, there is much less disagreement between models, and again both agree within the uncertainty of the data-based estimate. The meridional structure of the bomb $\Delta^{14}C$ inventory also differs very little between the models and the data-based estimate (Fig. 9). On the other hand, the meridional structure of anthropogenic CO_2 inventory differs much more between models and the data-based estimate (Fig. 10). In the southern extratropics, the eddying model's inventory is 26% less than that in the noneddying model, which is greater in magnitude than the 18% reduction in global inventory. As for CFC-11, the eddying model also generally captures the magnitude and pattern of the data-based estimates for anthropogenic DIC, despite some disagreement in the tropical and subtropical Pacific Ocean as well as south of the SAF. In those high southern latitudes, the eddying model underestimates the data-based estimates for anthropogenic DIC (Key et al., 2004; Sabine et al., 2004),

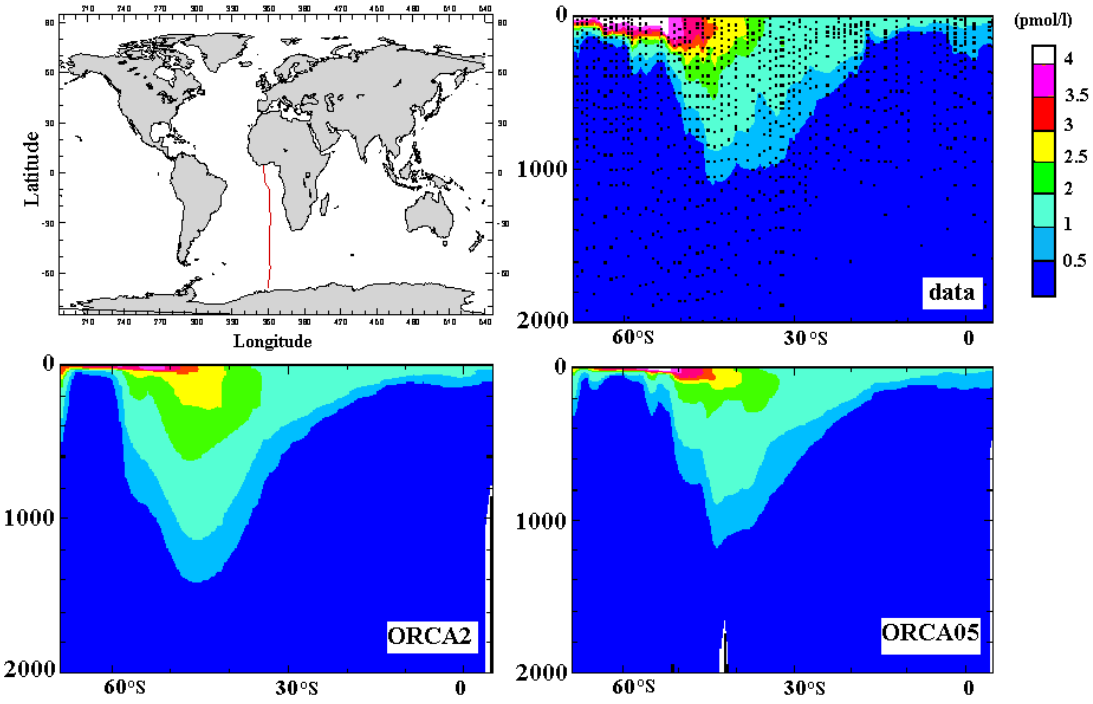

Fig. 7. CFC-11 concentration (in pmol l^{-1}) along the AJAX section (0° E, 1983) as observed and simulated by the noneddying (ORCA2) and the eddying (ORCA05) model.

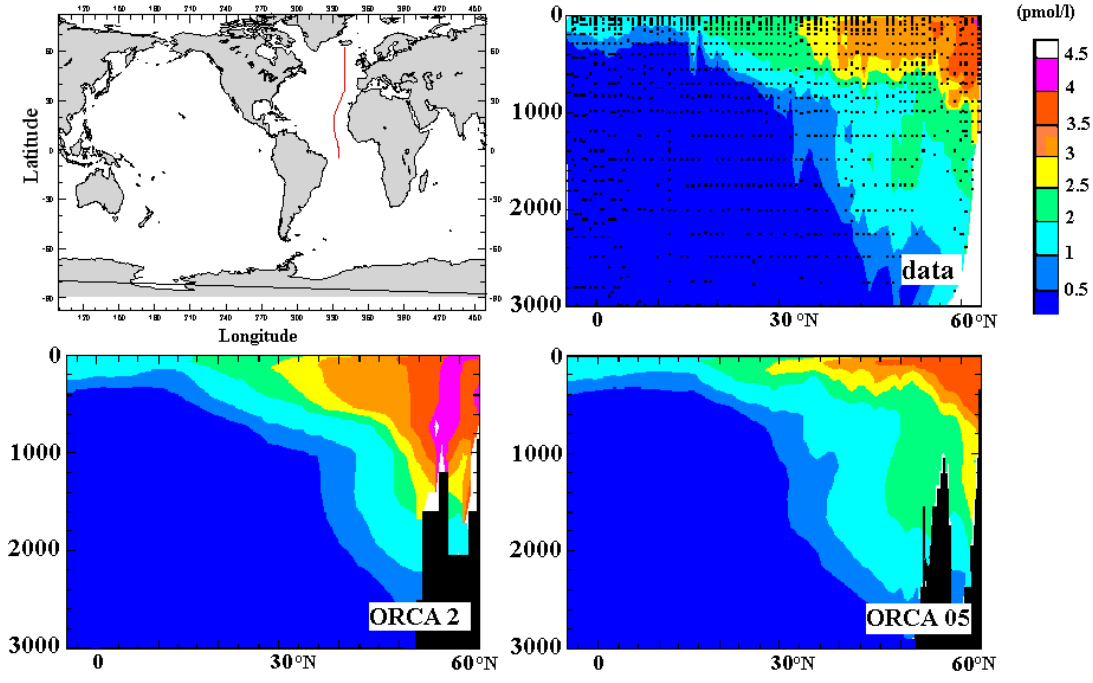

Fig. 8. CFC-11 concentration (in pmol l^{-1}) along the Na20w section (1993) as observed and simulated by the noneddying (ORCA2) and the eddying (ORCA05) models

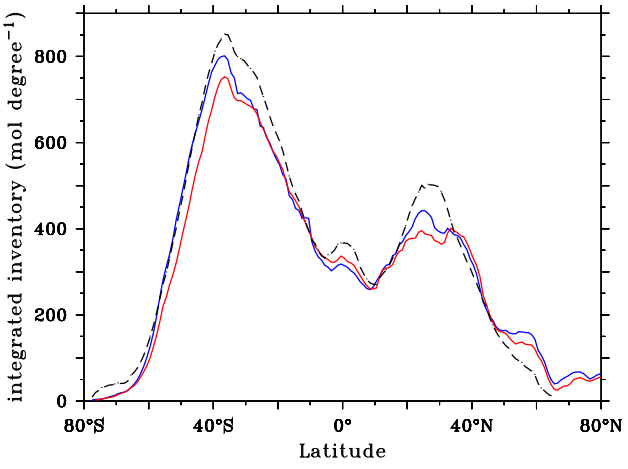

Fig. 9. Global zonal integral of the bomb $\Delta^{14}C$ inventory as observed (black dashes, GLODAP) and as simulated by the noneddying (blue) and eddying (red) models at end of year 1994.

partly because the mixed-layer depth is too shallow (Fig. 4) as discussed already for the same deficiency that was revealed by CFC-11.

Unfortunately, systematic errors in the data-based estimates for anthropogenic DIC (Matsumoto and Gruber, 2005) compromise our ability to use that tracer by itself as a reference to validate models (Orr et al., 2001). Anthropogenic DIC is clearly not of the same value as CFC-11, which is measured directly. Yet, trends for anthropogenic DIC are similar to those for CFC-11, i.e., in terms of the systematic differences between the models and the data reference. This would be expected if the data-based estimates for anthropogenic DIC were roughly correct. In any case, throughout the southern extratropics there are striking differences between the noneddying and eddying models for both CFC-11 and anthropogenic DIC; for both tracers, the eddying model is much closer to the data reference. Having studied how each tracer is affected by improved resolution, we now turn our attention to how the three tracers differ in terms of ocean uptake, inventory, and northward transport.

3.2 Tracer-tracer differences

3.2.1 Ocean uptake

Figure 11a shows the zonal integrals of the cumulative fluxes for the three tracers obtained using the noneddying model. Cumulative fluxes are calculated as the time-integrated air-to-sea fluxes since the beginning of the simulations, and for comparison they are normalised by dividing by the total global uptake. Although all three tracers exhibit maximum uptake between 40° S and 50° S, the relative amount that is taken up south of 20° S varies: 65% for CFC-11, 56% for anthropogenic CO_2, and 50% for bomb $\Delta^{14}C$. These dissim-

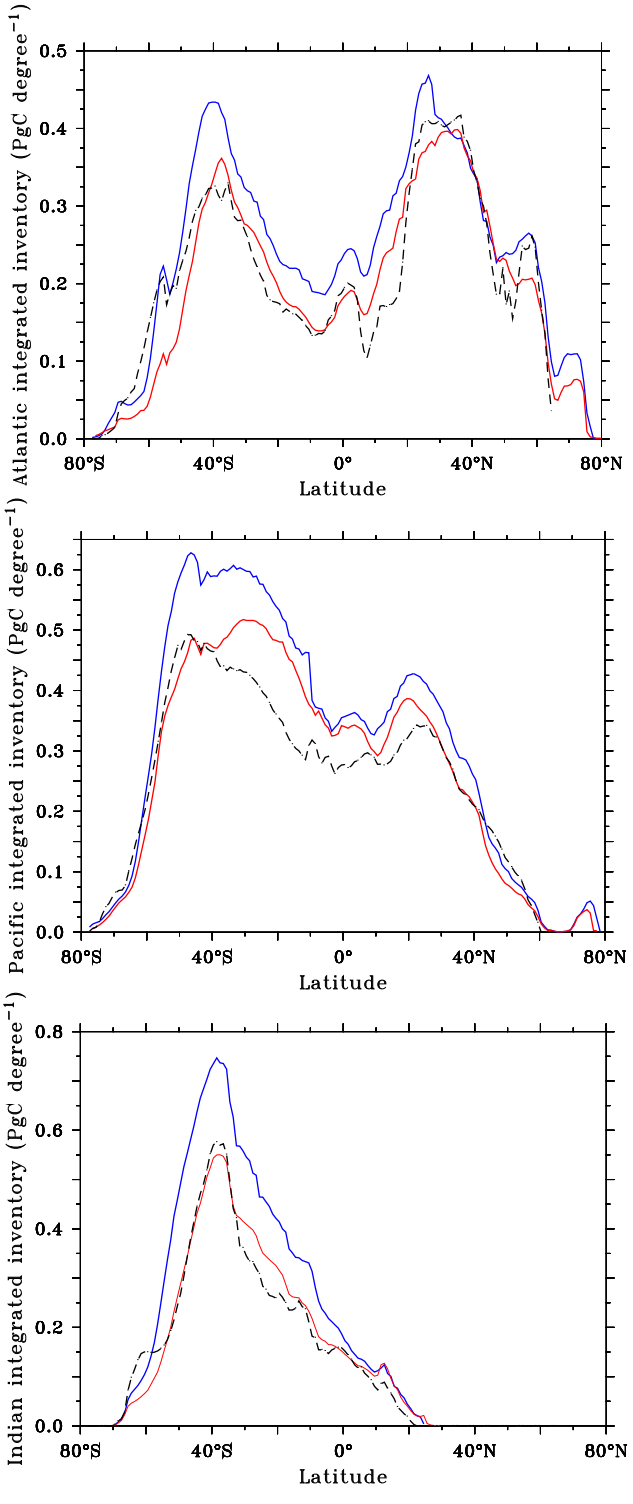

Fig. 10. Inventories of anthropogenic CO_2 at the end of 1994 integrated zonally over each of the Atlantic (top), Pacific (middle), and Indian (bottom) basins for the data-based estimates (black dashes, GLODAP) as well as the noneddying (blue) and eddying (red) models.

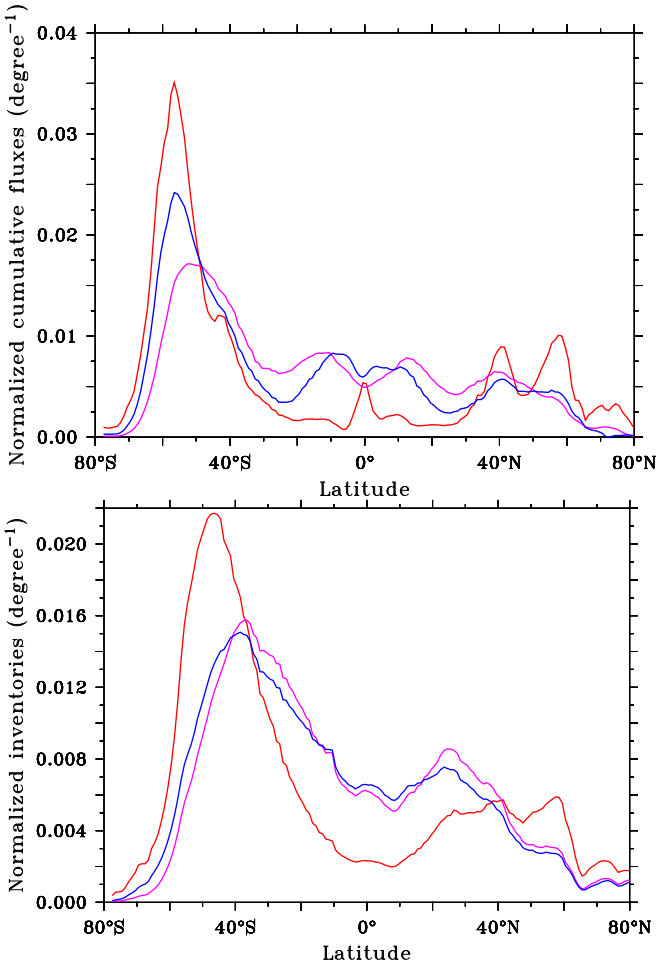

Fig. 11. Zonal integral of the normalised cumulative fluxes (upper) and inventories (lower) of CFC-11 (red), anthropogenic CO_2, (blue) and bomb $\Delta^{14}C$ (purple) in the noneddying model at end of 1994. Cumulative fluxes and inventories were normalised by dividing by the total global uptake.

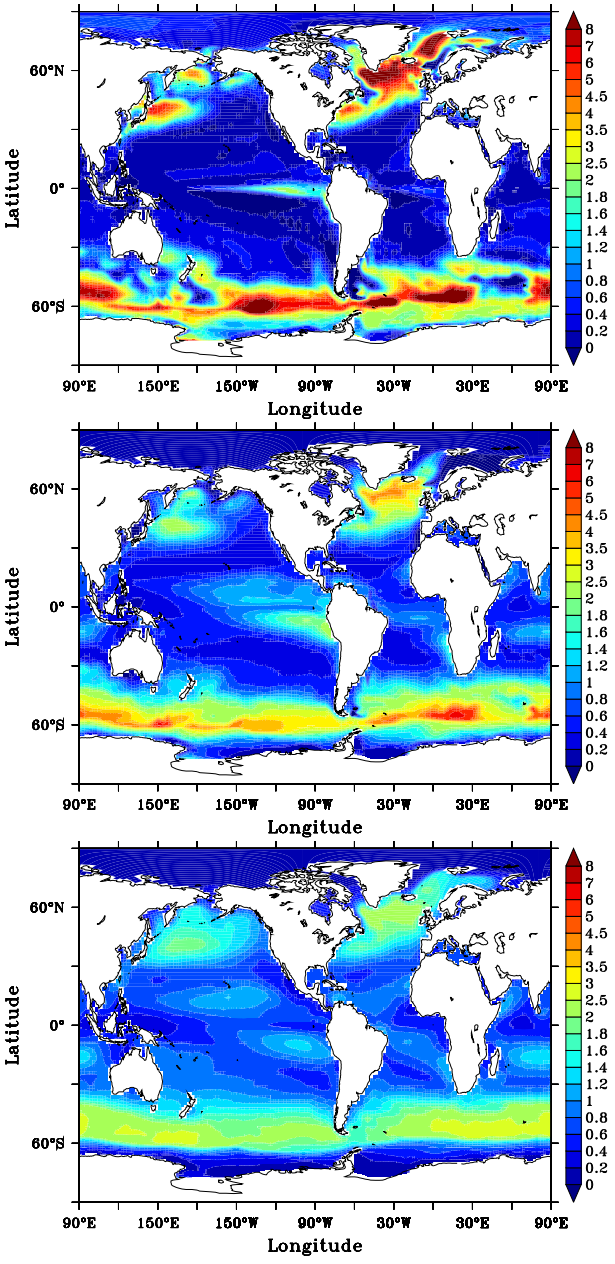

Fig. 12. Normalised cumulative fluxes simulated by the noneddying model for CFC-11 (upper), anthropogenic CO_2 (middle), and bomb $\Delta^{14}C$ (lower), accumulated since the beginning of each simulation until the end of year 1994. Fluxes were normalised by dividing each field by the global area-weighted mean flux; thus there are no units.

ilarities are due to the differences between the three tracers in terms of their air-sea equilibration times and atmospheric histories (i.e., different shapes and rates of change). When combined with local differences in stratification and surface-layer residence times, these lead to different tracer uptake patterns. Figure 12 presents the corresponding cumulative flux maps for the three tracers normalised by dividing each by its area-weighted average surface flux.

Clearly oceanic uptake is not distributed evenly over the different basins. For example, the Atlantic Ocean absorbs up to 39% of the total CFC-11 uptake, although it covers only 26% of the total ocean area. For the two anthropogenic carbon tracers, there are smaller contrasts in uptake between basins, with the relative contribution of the Atlantic Ocean shrinking to 30% for anthropogenic CO_2 and 27% for bomb $\Delta^{14}C$.

The air-sea fluxes of the three tracers also differ in their responses to increasing horizontal resolution (Fig. 13). The bomb $\Delta^{14}C$ uptake is nearly unchanged, both regionally and globally. In contrast, CFC-11 and anthropogenic CO_2 air-sea fluxes decrease by 28% and 25% in the southern extratropics and by 22% and 18% in the World Ocean. The reduction

Table 1. Changes in integrated global- and basin-scale, air-to-sea tracer fluxes when moving from the noneddying to the eddying model.

	CFC-11	CO_2	$\Delta^{14}C$
Atlantic	–34%	–21%	–4%
Pacific	–10%	–12%	–4%
Indian	–23%	–24%	–6%
South of 20° S	–28%	–25%	–7%
South of 50° S	–19%	–23%	–6%
Global	–22%	–18%	–5%

Table 2. Changes in integrated basin-scale tracer inventories when moving from the noneddying to the eddying model.

	CFC-11	CO_2	$\Delta^{14}C$
Atlantic	–23%	–18%	–6%
Pacific	–11%	–14%	–2%
Indian	–37%	–25%	–7%
South of 20° S	–31%	–26%	–9%
South of 50° S	–44%	–35%	–14%
Global	–22%	–18%	–5%

of the air-sea CFC-11 flux is largest in the Atlantic Ocean (34%), moderate in the Indian (23%), and weakest in the Pacific (∼10%). Discrepancies between basins are less important for the air-sea flux of anthropogenic CO_2 (Table 1). In both model versions, the peak uptake for CFC-11 remains south of 58° S and that for bomb $\Delta^{14}C$ remains at 52° S; conversely, the peak uptake for anthropogenic CO_2 shifts from 57° S to 54° S with the increase in horizontal resolution (Fig. 13). Later we show that this shift in the peak for anthropogenic CO_2 also affects its northward transport.

3.2.2 Inventories

Figure 11b shows each tracer's normalised zonal integral inventory in the coarse-resolution model. More than 62% of the global inventory of CFC-11 is stored south of 20° S, whereas only 49% of total uptake of anthropogenic CO_2 and 47% of bomb $\Delta^{14}C$ are stored in this same region. That is, the relative contribution of the southern extratropical to the total air-sea flux is larger for CFC-11 than for the two other tracers (Fig. 11a).

Maps of these quantities (Fig. 14) reveal that the highest specific inventories (i.e., mass per unit area) for CFC-11 are found in the North Atlantic and between 30° S and 50° S. For the other tracers, the Atlantic Ocean also exhibits the highest specific inventories, but the contrast between basins is less for anthropogenic CO_2 and less still for bomb $\Delta^{14}C$. As for the vertical distributions, nearly 80% of the total anthro-

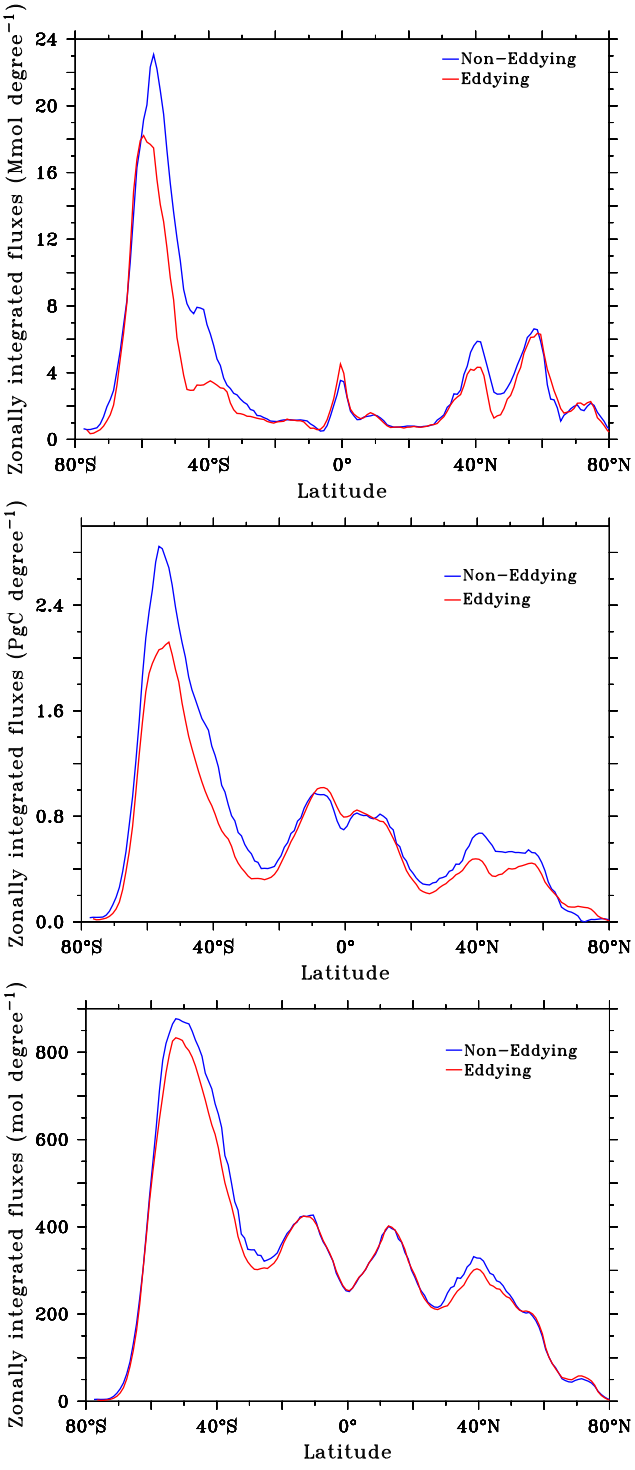

Fig. 13. Zonal integrated cumulative fluxes at the end of 1994 for CFC-11 (upper), anthropogenic CO_2 (middle), and bomb $\Delta^{14}C$(lower) simulated by the noneddying (blue) and eddying models (red).

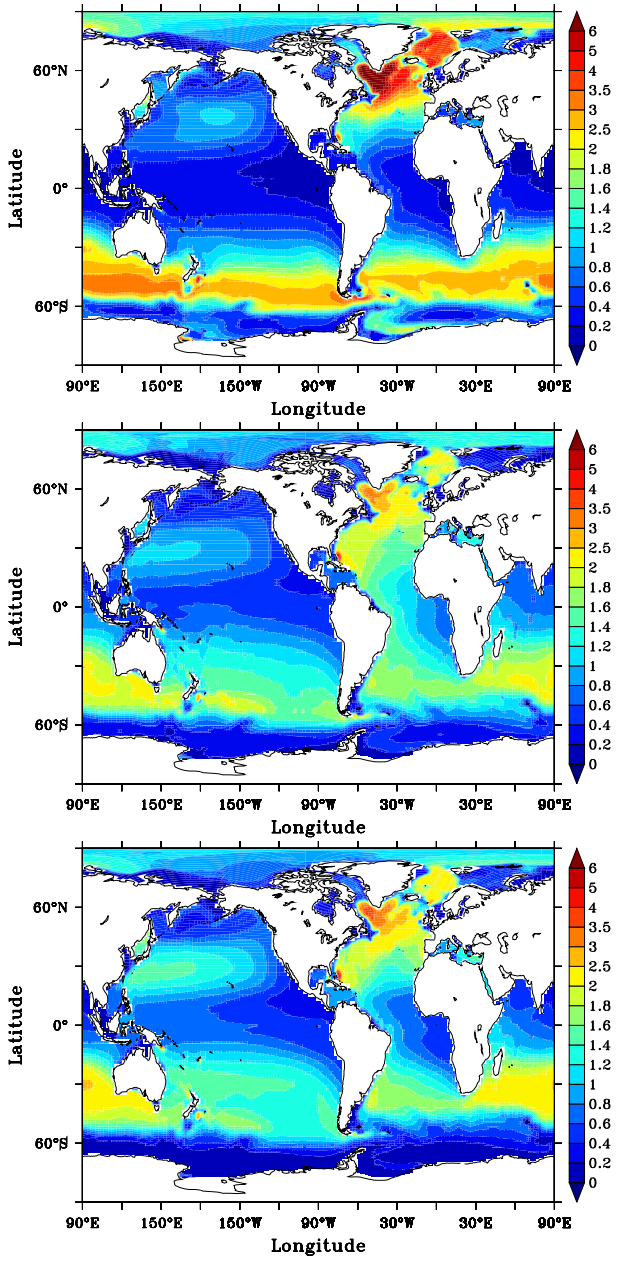

Fig. 14. Normalised inventories simulated in the noneddying model obtained by dividing by the mean area-weighted inventory for CFC-11 (top), anthropogenic CO_2 (middle), and bomb $\Delta^{14}C$ (bottom) at end of year 1994.

pogenic CO_2 and around 90% of CFC-11 and bomb $\Delta^{14}C$ that is taken up by the ocean is stored in the upper 1000 m. Thus the large majority of the total inventory of these transient tracers are confined above the thermocline. The only place where large tracer concentrations penetrate to mid and abyssal depths is in the North Atlantic as a result of the formation of the North Atlantic Deep Water (NADW). These findings are consistent with previous observational studies (Sabine et al., 2004; Willey et al., 2004). Thus our analysis remains focused on the upper and intermediate ocean.

Table 3. Global inventories of the three transient tracers from the data-based estimates (Key et al., 2004; Willey et al., 2004; Sabine et al., 2004) and as simulated by ORCA2, ORCA05, and the eddy resolving model from Sasai et al. (2004).

	CFC-11 (10^6mol)	CO_2 (Pg C)	$\Delta^{14}C$ (10^{28}atoms ^{14}C)
ORCA2 (noneddying)	648	120	3.07
ORCA05 (eddying)	506	98	2.94
GLODAP	544 (±81)	106 (±16)	3.13 (±0.47)
Willey et al. (2004)	550	–	–
Sasai et al. (2004)	510	–	–
Sabine et al. (2004)	–	106	–

The decrease in air-sea fluxes of CFC-11 and anthropogenic CO_2 that accompanies increased horizontal resolution leads to equivalent reductions in the global tracer inventories of these two tracers. Yet, this global decrease does not occur homogeneously throughout the three basins (Table 2). With increased resolution, both tracers show nearly the same decreases in uptake and storage in the Pacific Ocean. In contrast, the reduction in storage is more pronounced in the Indian Ocean and less pronounced in the Atlantic Ocean relative to the reduction in uptake. Thus higher model resolution leads to greater lateral export of CFC-11 and anthropogenic CO_2 from the Indian to the Atlantic Ocean. It is well known that heat and mass are exchanged between these two basins mainly via the Agulhas Current and the Antarctic Circumpolar Current (ACC), each of which is characterised by high eddy activity (Gordon, 1986; Rintoul, 1991). We hypothesise that the eddying model's lower Indian-to-Atlantic net export of CFC-11 and anthropogenic CO_2 result from some combination of stronger Agulhas transport and weaker ACC transport. Both effects are known to be induced by eddies (Hallberg and Gnanadesikan, 2001). Thus, eddies play a role in the inter-basin transport of transient tracers. One might also expect that eddies contribute to meridional transport of transient tracers.

3.2.3 Northward transport

To detail meridional or northward transport of a transient tracer, we first computed tracer divergence as the zonal integral of the difference between cumulative flux and column inventory. Positive divergence (Flux – Inventory) indicates areas of tracer export or loss; negative divergence indicates areas of tracer gain. Both are due to meridional transport. The integral of the tracer divergence from south to north is the time-integrated northward transport since the beginning of simulation (Fig. 15).

For bomb $\Delta^{14}C$, the meridional distribution of the northward transport is nearly the same for the two versions of

the model. Yet for CFC-11, there is a decrease of equatorward transport in the Northern Hemisphere between 0° N and 45° N, which is largest at 35° N. In contrast, in the southern extratropics, meridional transport of CFC-11 changes little with improved horizontal resolution. For anthropogenic CO_2, the decreased equatorward transport due to increased horizontal resolution is a general feature that occurs in both the Southern and the Northern Hemispheres, between 60° S and 50° N. These discrepancies between tracers result from their contrasting vertical distributions in the upper ocean. For example, the horizontal gradients of anthropogenic CO_2 and of CFC-11 are of opposite signs within the thermocline (see Sect. 4.3). Gaining more insight into the exact mechanisms that drive these contrasts requires further study, which we leave for future work.

4 Discussion

For insight into how mesoscale eddies affect transient tracer distributions, we explored the main differences between the dynamics of the eddying and the noneddying simulations.

4.1 Eddies and stratification

In the higher southern latitudes, the simulated mixed layer is generally shallower in the eddying model (Fig. 4). The largest differences are found in the Indian and Atlantic basins between 40° S and 60° S, where the winter mixed layer in the eddying model is locally 200 to 300 m shallower than in the noneddying model. Relative to the observations between 40° S and 50° S (de Boyer Montégut et al., 2004), the simulated mixed layers are too deep in both models, particularly for the noneddying model in the Indian Ocean (de Boyer Montégut et al., 2004). The eddying model's increased horizontal resolution substantially reduces the spurious wintertime convection in the higher southern latitudes. This reduction, due to explicitly including mesoscale eddies, is consistent with previous findings for the effect of Gent & McWilliams eddy parameterisation (Gent and McWilliams, 1990; Gent et al., 1995) on the strength of wintertime convection in the high southern latitudes (Hirst and McDougall, 1996; England and Hirst, 1997). Because convection is tied to water column stratification, we may anticipate that there are major changes in stratification between the two experiments. Indeed, increased resolution changes simulated subsurface density between 60° S and 40° S by flattening isopycnal surfaces. That flattening strengthens upper ocean stratification and yields a more realistic vertical density structure in the high southern latitudes. More specifically, baroclinic mesoscale eddies serve to release Available Potential Energy (APE) of the mean flow in the form of Eddy Kinetic Energy (EKE), thereby reducing the baroclinic instability and ensuring a more stable stratification. Marshall et al. (2002) also showed with idealised numerical experiments that mesoscale

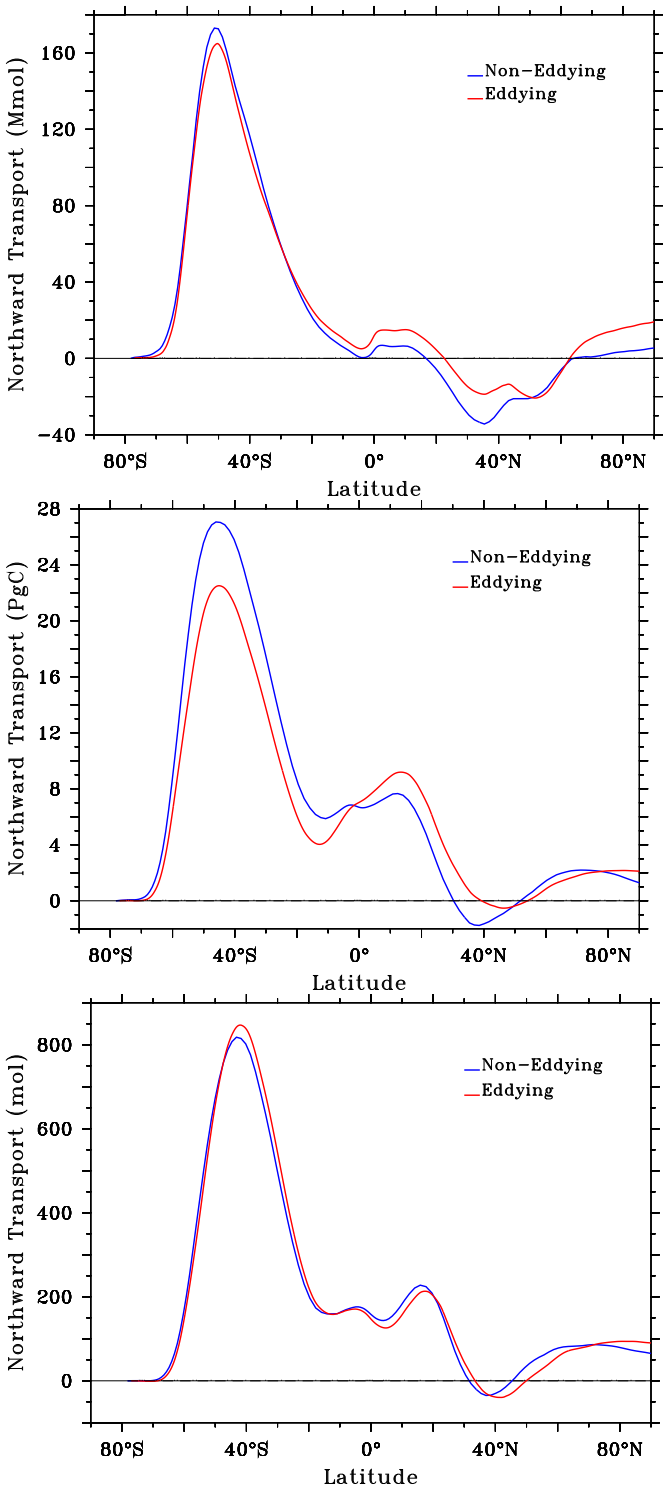

Fig. 15. Total northward transport of CFC-11 (top), anthropogenic CO_2 (middle), and bomb $\Delta^{14}C$ (bottom) since the beginning of each simulation until 1994 as simulated by the noneddying (blue) and the eddying (red) models at end of year 1994.

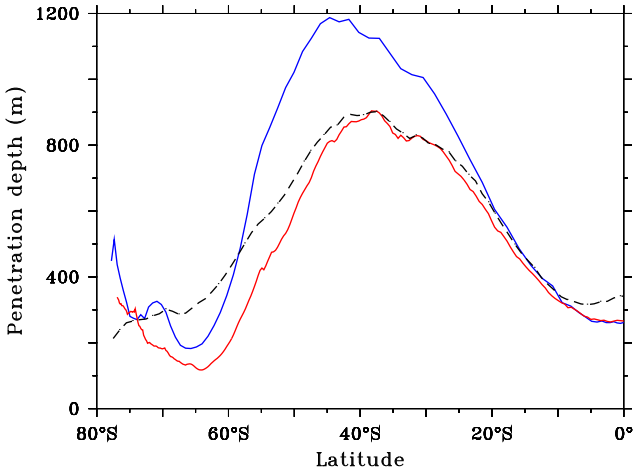

Fig. 16. Zonal mean of CFC-11 penetration depth [m] as observed (black dashes, GLODAP) and as simulated by the noneddying (blue) an eddying (red) models over the Southern Hemisphere. The penetration depth of a tracer is defined as the tracer inventory [mol m^{-2}] divided by its surface concentration [mol m^{-3}].

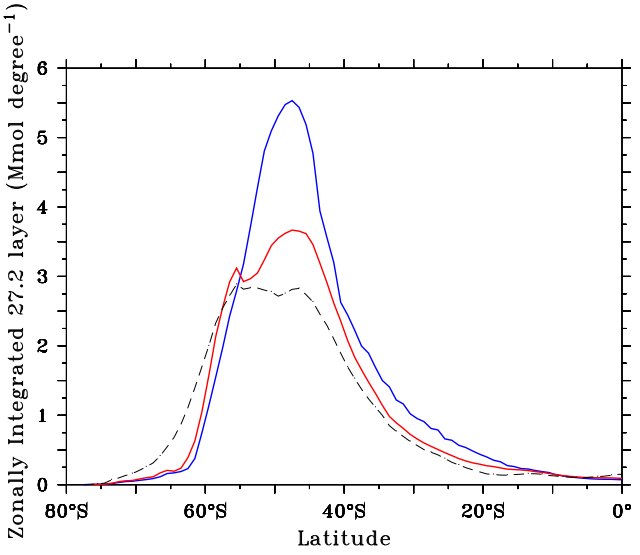

Fig. 17. Zonal integral of CFC-11 inventory (10^6mol) in the AAIW, defined as the 27.0–27.4 σ_0 layer as observed (black dashes, GLODAP) and as simulated by the noneddying (blue) and the eddying (red) models.

eddies play a key role in setting up the stratification. By strengthening vertical stratification in the high southern latitudes, mesoscale eddies affect the rate at which the thermocline and intermediate waters are ventilated as well as how water masses are transformed within the upper ocean. As a consequence of the flattening of density surfaces, vertical penetration of CFC-11 and anthropogenic CO_2 are reduced in the eddying model (Fig. 16).

4.2 Ventilation and upper water mass transformation

Higher resolution and thus the presence of mesoscale eddies reduces the excessive vertical penetration of simulated CFC-11 between 60° S and 40° S (Fig. 6). For example, between 55° S and 50° S, waters at 1000 m contain more than 2 pmol l^{-1} of CFC-11 in the noneddying model but only around 0.5 pmol l^{-1} in the eddying model (as in the observations). Most of the CFC-11 that penetrates into subsurface waters south of 40° S is carried by Subantarctic Mode Water (SAMW) and Antarctic Intermediate Water (AAIW) as they subduct near the SAF. In the SAMW layer (σ_0=26.5 to 27.0), the CFC-11 inventory between 60° S and 40° S is nearly twice that in the AAIW layer (σ_0=27.0 to 27.4). Yet that SAMW inventory is only 2% less in the eddying model relative to the noneddying model, whereas the corresponding inventory reduction in the AAIW is 20%. Thus we focus on the AAIW. That intermediate water is easily identified as a tongue of fresh water with a salinity minimum of 34.2 and a mean potential density of ∼27.2. The AAIW extends northward from the Antarctic Polar Frontal Zone (APFZ), which is located near the Antarctic Divergence along the southern flank of ACC, to intermediate depths at subtropical latitudes. The AAIW's CFC-11 inventory (Fig. 17) illustrates that the noneddying model's excessive ventilation of that water mass is responsible for much of the excessive vertical penetration of transient tracers in the southern extratropics. The noneddying model overestimates the AAIW's observed CFC-11 content in all basins, particularly in the Atlantic and in the Indian sectors of the Southern Ocean, where the excess reaches more than a factor of two. The 20% reduction in the AAIW's CFC-11 inventory between 60° S and 40° S is accompanied by decreases in the total volume of the AAIW layer, by 33% between 60° S and 50° S and by 19% between 50° S and 40° S. Thus, the strong ventilation of the upper and the intermediate ocean in the southern extratropics in the noneddying model is partly linked to its excessive AAIW formation rate.

To better understand the source of AAIW, the meridional circulation, and the water mass transformations that occur in upper waters (above the permanent thermocline) between 40° S and 65° S, we calculated the isopycnal transport streamfunction in both the eddying and noneddying versions of the model. Averaging along density instead of depth coordinates avoids the spurious large apparent diapycnal motion in the upper Southern Ocean known as the Deacon Cell (Döös and Webb, 1994). When the isopycnal streamfunction is given on neutral density surfaces, McIntosh and McDougall (1996) showed that it approximates the so-called residual mean circulation, which is the sum (calculated in depth coordinates) of the Eulerian circulation and the eddy-induced flow (Andrews and McIntyre, 1976; Holton, 1981). Near the ocean surface, where eddies are most active, neutral surfaces are tangential to σ_0 potential density surfaces (McDougall, 1987). Following the lead of (Döös and Webb, 1994), we computed the isopycnal streamfunc-

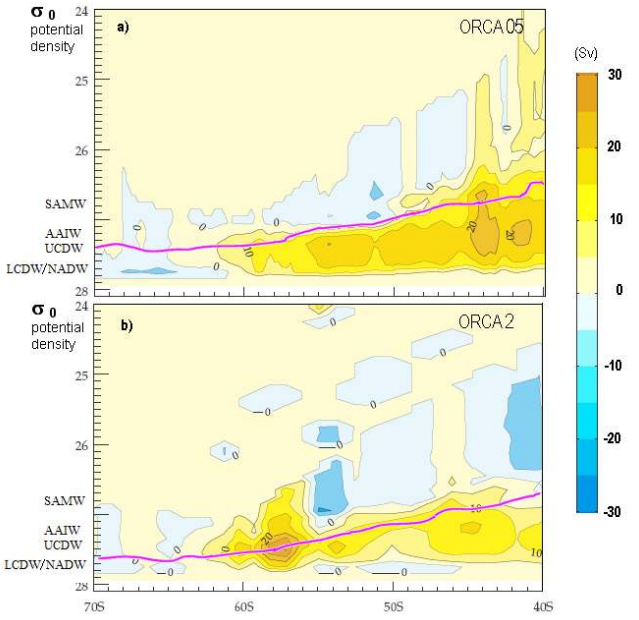

Fig. 18. The isopycnal transport streamfunction (in Sv) plotted in σ_0 coordinate for the noneddying (ORCA2) and eddying (ORCA05) models for the region south of 40° S. The contour interval is 5 Sv. The purple line indicates the position of the annual maximum mixed layer depth in density space. Positive values indicate clockwise circulation.

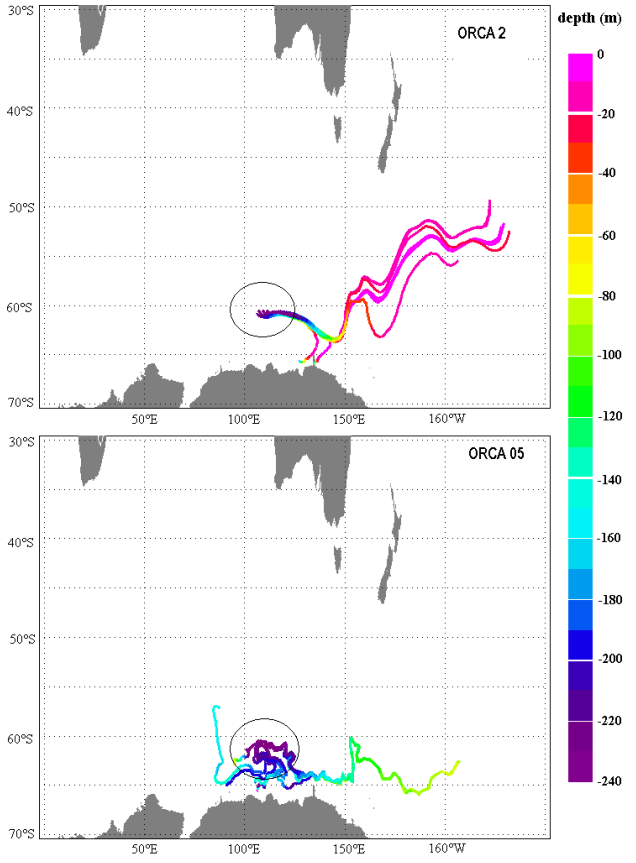

Fig. 19. Four-year trajectories of 10 particles launched from 250 m at 60° S, between 110° E and 120° E. Colours represent the depth of the particles.

tion relative to the surface (σ_0) by projecting model output onto 72 evenly spaced potential density layers ranging from 21 to 28 (Fig. 18). Yet, due to compressibility effects, deeper water masses, including the Lower Circumpolar Deep Water (LCDW), NADW, and AABW, are not well defined by σ_0. Thus a σ_0-based separation between NADW and LCDW would be misleading. Here we consider these denser water masses as a unique layer (27.6–28.1 density class).

In the noneddying simulation, the residual circulation in the upper ocean south of 40° S is characterised by a small Deacon Cell with a maximum of 30 Sv at 58° S near the Antarctic Divergence. Although unrealistic, such large meridional circulation is not surprising given that this model has no eddies, which in the real ocean counter part of the Ekman driven transport. In an observational study, Karsten and Marshall (2002) found a northward Ekman driven transport of more than 23 Sv between 51° S and 57° S. The equivalent northward transport in our noneddying model is associated with excessive upwelling of about 26 Sv of dense water (27.6–28.1) that is transported across the 27.5 surface between 65° S and 58° S. Most of this water that feeds the AAIW formation lies within the "bowl", which separates the subsurface ocean from the interior ocean (Marshall and Nurser, 1992), thereby directly ventilating the upwelled dense waters. Therefore, the excessive upwelling rate is closely linked to the overestimation of AAIW ventilation in the noneddying version of the model.

In the eddying simulation, due to the countering effect of eddy-induced transport, the Deacon Cell nearly disappears and the residual circulation is roughly halved to 14 Sv of northward near-surface transport between 55° S and 60° S. Consequently, the upwelling of the dense water masses along the southern flank of the ACC is substantially reduced. In the eddying model only 12 Sv is upwelled across the 27.5 σ_0 surface between 65° S and 58° S. This model result is consistent with the observational study of Karsten and Marshall (2002) who found a residual circulation of about 13 Sv at 57° S. The large reduction in upwelling of denser, tracer-impoverished waters results in an equally large decrease in AAIW ventilation (Fig. 17). Additionally, Fig. 18 reveals that the diapycnal flux diminishes with increased resolution as the isopycnal overturning streamlines become flatter. This makes sense given that eddies facilitate meridional circulation along isopycnal surfaces (Hallberg and Gnanadesikan, 2001). These eddy-induced reductions in water mass transformation within the upper waters of high southern latitudes lead to reduced air-sea fluxes of transient tracers, as detailed below.

4.3 Surface water saturation and residence time

Within the surface and intermediate waters of the southern high latitudes, eddies act to weaken the residual circulation, which is northward at the surface. To illustrate this eddy-induced slowdown of the residual circulation south of 40° S, we examined the Lagrangian trajectories of individual particles that were launched from under the mixed layer of the upwelling region south of the ACC. For this analysis, we relied on the Lagrangian diagnostic tool ARIANE (Blanke and Raynaud (1997), which is fully documented at http://fraise.univ-brest.fr/~blanke/ariane/doc.html). Figure 19 shows 4-year trajectories of particles launched from just below the mixed layer in the Indian Ocean at 60° S between 140° E and 120° E. In the noneddying model, water parcels upwell to the surface and are rapidly transported northward across the ACC, whereas in the eddying model they spend more time in the mixed layer before they are transported northward. Thus with higher resolution, there is an increase in the residence time of water parcels at the surface in the southern high latitudes where air-sea tracer fluxes are largest. Consequently, tracers have more time to accumulate in surface waters between 60° S and 40° S. For tracers whose equilibration times are relatively short (CFC-11 and anthropogenic CO_2), surface water concentrations increase and become closer to equilibrium with the atmosphere (Fig. 20). For example, at 53° S the magnitude of the air-sea difference in the partial pressure of CFC-11 in the eddying model is only half that in the noneddying model. This reduction along with the reduced upwelling of tracer impoverished waters from below explains why the increased resolution reduces cumulative air-sea fluxes of CFC-11 and anthropogenic CO_2.

On the other hand, ^{14}C's slow air-sea equilibration time of ~6 years is too long, relative to the increase in residence time of surface waters, to allow surface-water levels of bomb Δ^{14}C to become as close, relatively speaking, to the atmospheric level. For example, the average level of bomb Δ^{14}C in the atmosphere over the southern extratropics was at 144 permil in 1994. Refining resolution increased surface-ocean bomb Δ^{14}C from 61 to 69 permil at 53° S (Fig. 21). This represents only a 10% reduction in the air-sea difference for bomb Δ^{14}C (i.e., $C_a - C_o$ in Eq. (5)), which is much less than the 50% reduction for the air-sea difference in the partial pressure of CFC-11 mentioned above. The small relative decrease in the air-sea difference for bomb Δ^{14}C at 53° S is comparable in magnitude to the corresponding reduction in the bomb Δ^{14}C flux in the same area (Table 1), i.e., near where fluxes are largest. Despite its differences, bomb Δ^{14}C is carried by the same circulation and is submitted to the same vertical mixing as the two other anthropogenic tracers. Eddy-induced changes in vertical mixing within the ocean interior affect the vertical distributions of all three tracers. Below the thermocline, concentrations of all three tracers decrease (Fig. 21) because as the resolution is refined, the water column becomes more stratified. Thus, enhancing resolution decreased vertical penetration of all three tracers (Fig. 21).

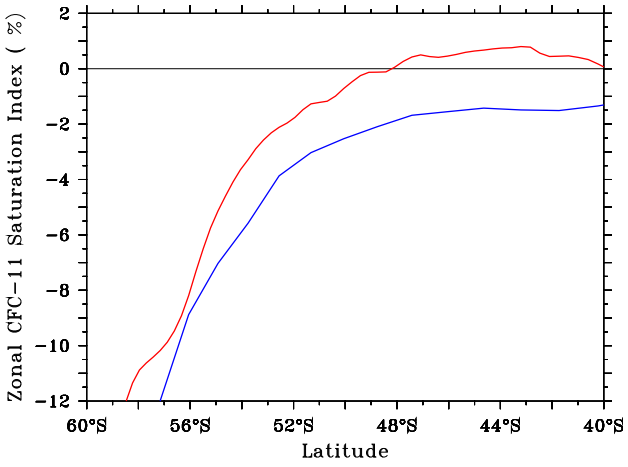

Fig. 20. Zonal mean of the CFC-11 saturation index in the Atlantic between 60° S and 40° S for the noneddying (blue) and eddying (red) models. The CFC-11 saturation index is defined as: $SI = 100 \times (\frac{p_o - p_a}{p_a})$, where p_o and p_a are CFC-11 partial pressures at ocean surface and in the atmosphere respectively.

In the previous analysis, we highlighted the role of contrasting equilibration times between the three tracers to explain why the bomb Δ^{14}C behaves so differently from the two other tracers. Additionally, the three tracers differ in terms of the shape of their atmospheric history (Fig. 22). To discriminate between these two factors, we made another type of ^{14}C simulation, where instead of the nuclear-era perturbation, we accounted for only the Suess effect, i.e., the reduction in the atmospheric $^{14}C/^{12}C$ ratio due to the emission of fossil CO_2 during the industrial era. This perturbation simulation for the Δ^{14}C Suess-effect was made in both models over most of the industrial era, from 1839 to 1950, just prior to the beginning of the nuclear-era increase in atmospheric CO_2. Although the air-sea equilibration time for this Δ^{14}C Suess effect is identical to that for bomb Δ^{14}C, the corresponding atmospheric histories are radically different. As opposed to the bomb pulse input, the Suess effect Δ^{14}C exhibits a slow atmospheric decrease, similar in form to the anthropogenic CO_2 increase. In this way, we isolated the effect of the Δ^{14}C time history. The magnitude of the Suess Δ^{14}C perturbation that is absorbed by the global ocean is 8% less in the eddying model relative to that in the noneddying model, whereas the corresponding difference is only 5% for bomb Δ^{14}C in 1994. Although this 8% change for the C-14 Suess effect is larger than that for bomb Δ^{14}C, it still remains less than 1/3 of that for anthropogenic CO_2 and CFC-11. Therefore, the atmospheric history does matter, but the main reason why bomb Δ^{14}C's response to increasing resolution is so much weaker than for the other two tracers is due to its much longer air-sea equilibration time.

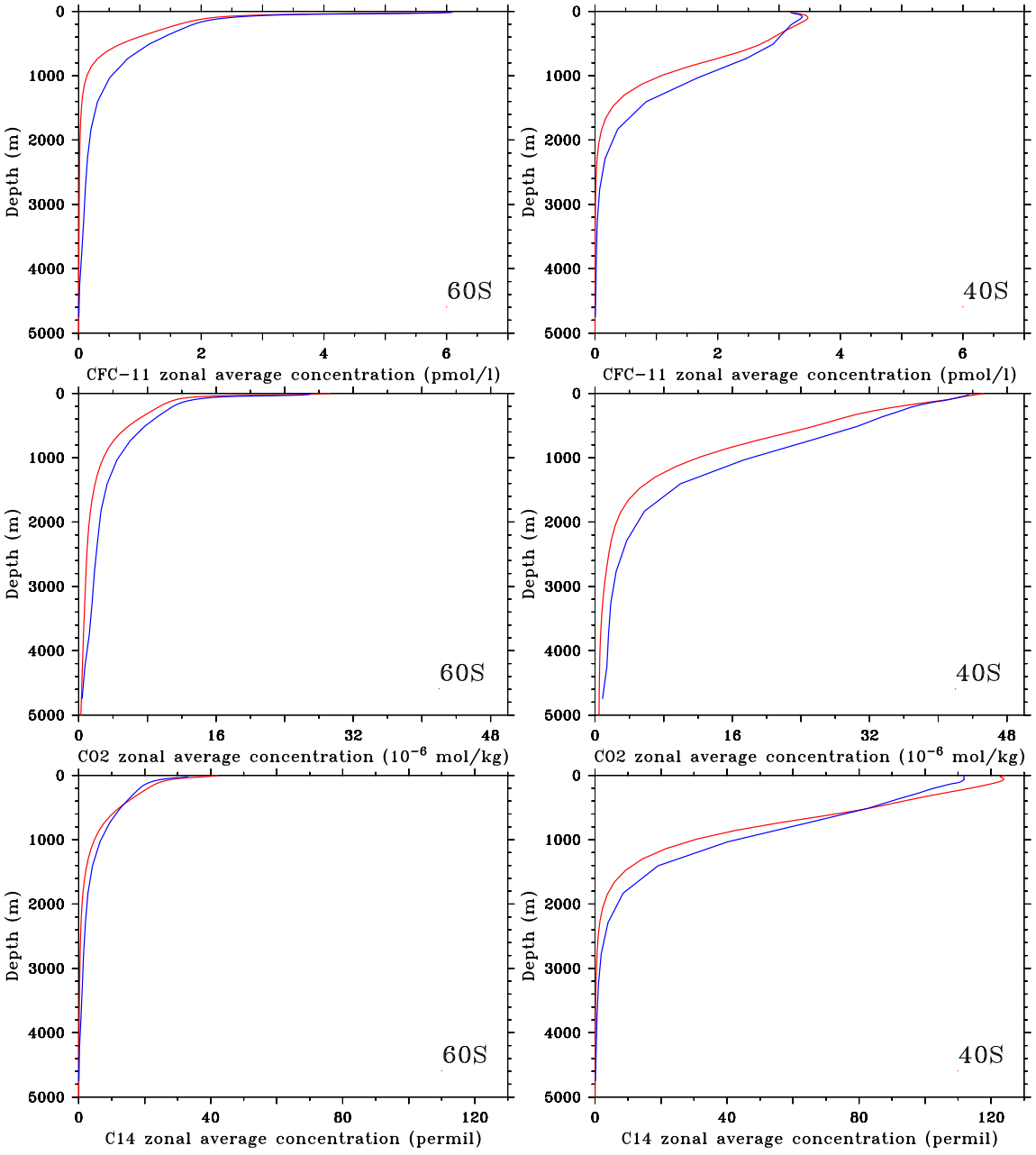

Fig. 21. Vertical profiles of zonally averaged concentrations of CFC-11 (upper), anthropogenic DIC (middle), and bomb Δ^{14}C (lower) at 60° S (left) and 40° S (right) for the noneddying (blue) and eddying (red) models.

5 Summary and conclusions

The effect of mesoscale eddies on global distributions of CFC-11, anthropogenic CO_2, and bomb Δ^{14}C was investigated by comparing eddying and noneddying versions of the same coupled ocean-sea ice model ORCA-LIM. Our aim was to evaluate how explicitly simulating eddies affects three complementary anthropogenic tracers, particularly in the southern extratropics where ocean uptake, storage, and meridional transport of these tracers are largest.

Comparable simulations with noneddying and eddying versions of the same model showed that the improved resolution led to reductions in global ocean tracer uptake, by 22% for CFC-11 and by 18% for anthropogenic CO_2. The largest discrepancies occur in the Atlantic and Indian sectors of the southern extratropics. Conversely, eddies have little effect on global and regional bomb Δ^{14}C uptake. By comparing basin-integrated cumulative fluxes and inventories, we found that eddies also affect inter-basin tracer exchange of CFC-11

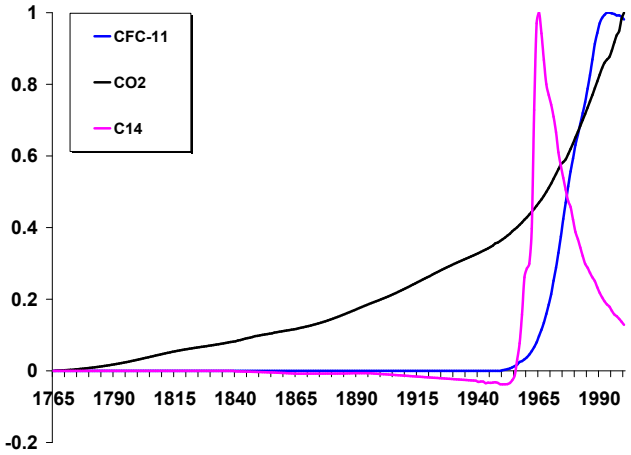

Fig. 22. Atmospheric histories of CFC-11 (blue), anthropogenic CO_2 (black), and $\Delta^{14}C$ (purple) over the prenuclear (prior to 1954) and nuclear or "bomb" (after 1954) periods. For comparison, each of the three curves was normalised by dividing by its maximum tracer concentration; thus there are no units.

and anthropogenic CO_2, substantially reducing Atlantic-to-Indian Ocean tracer transport. Model-data comparison reveals that moving from noneddying to eddying resolution substantially improved model performance, whereas using the GM parameterisation with the noneddying model offered only limited improvement.

Secondly, we sought to improve the general understanding of the role of eddies in the high southern latitudes. Our results indicate that taking the first step towards higher resolution, moving from a coarse-resolution model to a model that begins to resolve mesoscale eddies, results in stronger upper ocean stratification in the high southern latitudes as manifested by a thinner mixed layer and flattened density surfaces. Eddies act to reduce AAIW-mediated ventilation of the intermediate waters, particularly in the Indian sector of the southern extratropics. By diagnosing the upper meridional circulation of the southern extratropics within an isopycnal framework, we showed that enhancing resolution to explicitly resolve mesoscale eddies decreases the AAIW formation rate in near-surface waters along the southern flank of ACC (at around 60° S). This leads to weaker ventilation of the thermocline and intermediate ocean. Eddies act to reduce the upwelling of dense water near the Antarctic Divergence (60° S–55° S), leading to a similar reduction in near-surface conversion of AAIW from 26 Sv in the noneddying model to 12 Sv in the eddying model at 58° S, in close agreement with the data-based estimate of Karsten and Marshall (2002).

Because eddies reduce meridional circulation (residual circulation) in the upper waters of the southern extratropics, they also bring surface-water levels of CFC-11 and anthropogenic CO_2 closer to those in the atmosphere, thereby reducing air-sea tracer fluxes. Refining resolution to explicitly simulate eddies increases surface residence time between 60° S and 50° S, where air-sea tracer fluxes are the largest, as illustrated by our Lagrangian trajectory analysis of particles launched from just below the mixed layer at 60° S in the upwelling zone of the Indian sector of Southern Ocean.

Unlike for CFC-11 and anthropogenic CO_2, bomb $\Delta^{14}C$ air-sea fluxes are much less sensitive to the eddy-induced slowdown in upper meridional circulation. The long air-sea equilibration time of bomb $\Delta^{14}C$ means it is slow to react during the relatively short period from when water masses are upwelled to the surface near the Antarctic Divergence until they are subducted a few degrees to the north near the SAF. Although the bomb $\Delta^{14}C$ inventory is nearly identical in both the noneddying and eddying models, vertical profiles of bomb $\Delta^{14}C$ in these models differ. Refined resolution increases concentrations near the surface and decreases concentrations deeper down owing to the eddying model's enhanced stratification and weaker ventilation of intermediate waters. Bomb $\Delta^{14}C$'s much weaker sensitivity to increased resolution is mainly due to its slower air-sea equilibration time, and not its pulse-shaped atmospheric history, as demonstrated by our sensitivity test for the preindustrial-to-prenuclear $\Delta^{14}C$ perturbation (Suess effect).

Despite similarities between these three anthropogenic tracers, their contrasting sensitivities to the mesoscale eddies reemphasise that we must be careful when trying to use findings from CFC-11 and bomb $\Delta^{14}C$ to make inferences about anthropogenic CO_2. We do not know if ocean model estimates of anthropogenic CO_2 would be altered substantially by further increases in horizontal resolution, but this study does emphasise the general need for ocean models to adopt higher resolution or improved subgrid-scale mixing parameterisations. For instance in climate models, higher resolution should likewise lead to more realistic ventilation of intermediate waters, which would alter decadal-scale ocean heat uptake.

Appendix A

Oceanic carbon perturbation δpCO_{2o} calculation

The equations used here are based on the perturbation approach of Sarmiento et al. (1992). The oceanic perturbation δpCO_{2o} is defined as the change in CO_2 partial pressure in the ocean from the beginning of the simulation (preindustrial level). The plot of $\frac{\delta pCO_{2o}}{\delta DIC}$ versus δpCO_{2o}, where δDIC is the concentration of dissolved inorganic carbon of the perturbation at the surface (in µmol kg^{-1}), reveals a linear relation for δpCO_{2o} ranging from 0 to 200 ppm. Thus, we can express simply the oceanic carbon perturbation as a function of δDIC by

$$\frac{\delta pCO_{2o}}{\delta DIC} = z_0 + z_1 \delta pCO_{2o} \quad \text{(A1)}$$

where z_0 and z_1 are seasonally varying coefficients depending on temperature T (in degrees Celsius) as in Sarmiento et al. (1995)

$$z_0 = 1.7561 - 0.031618 \times T + 0.0004444 \times T^2 \quad \text{(A2)}$$

$$z_1 = 0.004096 - 7.7086 \times 10^{-5} \times T + 6.10 \times 10^{-7} \times T^2 \quad \text{(A3)}$$

Rearranging Eq. (A1) and modifying to allow simulations to start at a different reference value than $pCO_{2a,\mathrm{ref}}$=280 ppm used in the original Siegenthaler and Joos (1992) equation for the perturbation approach gives

$$\delta pCO_{2o} = \frac{z_0[\delta\mathrm{DIC} + \delta\mathrm{DIC}_{\mathrm{corr}}]}{1 - z_1[\delta\mathrm{DIC} + \delta\mathrm{DIC}_{\mathrm{corr}}]} - pCO_{2a,\mathrm{corr}} \quad \text{(A4)}$$

with

$$\delta\mathrm{DIC}_{\mathrm{corr}} = \frac{pCO_{2a,\mathrm{corr}}}{z_0 + z_1 \times pCO_{2a,\mathrm{corr}}} \quad \text{(A5)}$$

and

$$pCO_{2a,\mathrm{corr}} = pCO_{2a,0} - pCO_{2a,\mathrm{ref}} = 278\,\mathrm{ppm} - 280\,\mathrm{ppm} \quad \text{(A6)}$$

Acknowledgements. We thank A.-M. Treguier, G. Madec, B. Barnier, and other DRAKKAR project members for discussions. We also thank S. Raynaud for his technical advice for using ARIANE and the ESOPA group at LOCEAN for the general support, improvements, and maintenance of the ocean model OPA-ORCA. Special thanks to GLODAP data providers. Support for this research has come from the French Commissariat à l'Energie Atomique (CEA) and the EU CARBOOCEAN Project (Contract no. 511176 [GOCE]). Computations were performed at CEA (CCRT) supercomputing centre. The IAEA is grateful for the support provided to its Marine Environmental Laboratory by the Government of the Principality of Monaco.

Edited by: V. Garcon

References

Andrews, D. and McIntyre, M.: Planetary waves in horizontal and vertical shear: The generalized Eliassen-Palm relation and the mean zonal acceleration, J. Atmos. Sci., 33, 2031–2048, 1976.

Arakawa, A.: Design of the UCLA general circulation model, numerical simulation of weather and climate, Tech. Rep. 7, University of California, Dept. of Meteorology, 1972.

Berliand, M. E. and Strokina, T.: Global distribution of the total amount of clouds (in Russian), Hydrometeorological Publishing House, Leningrad, Russia, 71 pp., 1980.

Blanke, B. and Delecluse, P.: Low frequency variability of the tropical Atlantic ocean simulated by a general circulation model with two different mixed layer physics, J. Phys. Oceanogr., 23, 1363–1388, 1993.

Blanke, B. and Raynaud, S.: Kinematics of the Pacific Equatorial Undercurrent: an Eulerian and Lagrangian approach from GCM results, J. Phys. Oceanogr., 27, 1038–1053, 1997.

Böning, C. and Budich, R.: Eddy dynamics in a primitive equation model: Sensitivity to horizontal resolution and friction, J. Phys. Oceanogr., 22, 361–381, 1992.

Broecker, W. S. and Peng, T.-H.: Gas exchange rates between air and sea, Tellus, 26, 21–35, 1974.

Chassignet, E. P. and Verron, J.: Ocean Weather Forecasting: An Integrated View of Oceanography, Springer, 2006.

Chelton, D. B., deSzoeke, R. A., Schlax, M. G., Naggar, K. E., and Siwertz, N.: Geographical variability of the first-baroclinic Rossby radius of deformation, J. Phys. Oceanogr., 28, 433–460, 1998.

Cox, M.: An eddy resolving model of the ventilated thermocline, J. Phys. Oceanogr., 15, 1312–1324, 1985.

Crosnier, L., Barnier, B., and Tréguier, A.: Aliasing of inertial oscillations in the 1/6° Atlantic circulation Clipper model : impact on the mean meridional heat transport, Ocean Model., 3, 21–32, 2001.

de Boyer Montégut, C., Madec, G., Fischer, A. S., Lazar, A., and Iudicone, D.: Mixed layer depth over the global ocean: an examination of profile data and a profile-based climatology, J. Geophys. Res., 109, C12003, doi:10.1029/2004JC002378, 2004.

Doney, S. and Bullister, J.: A chlorofluorocarbon section in the eastern North Atlantic, Deep-Sea Res., 39, 1857–1883, 1992.

Döös, K. and Webb, D. J.: The Deacon Cell and the other meridional cells in the Southern Ocean, J. Phys. Oceanogr., 24, 429–442, 1994.

Drijfhout, S.: Heat transport by mesoscale eddies in an ocean circulation model, J. Phys. Oceanogr., 24, 353–369, 1994.

Dutay, J.-C., Bullister, J., Doney, S. C., Orr, J. C., Najjar, R. G., Caldeira, K., Campin, J.-M., Drange, H., Follows, M., Gao, Y., Gruber, N., Hecht, M. W., Ishida, A., Joos, F., Lindsay, K., Madec, G., Maier-Reimer, E., Marshall, J. C., Matear, R., Monfray, P., Mouchet, A., Plattner, G. K., Sarmiento, J. L., Schlitzer, R., Slater, R. D., Totterdell, I. J., Weirig, M.-F., Yamanaka, Y., and Yool, A.: Evaluation of ocean model ventilation with CFC-11: Comparison of 13 global ocean models, Ocean Model., 4, 89–120, 2002.

England, M. H. and Hirst, A. C.: Chlorofluorocarbon uptake in a world ocean model 2. Sensitivity to surface thermohaline forcing and subsurface mixing parameterisation, J. Geophys. Res., 102, 15 709–15 731, 1997.

Enting, I., Wigley, T., and Heimann, M.: Future Emissions and Concentrations of Carbon Dioxide: Key Ocean/Atmosphere/Land Analyses, Tech. rep., CSIRO Division of Atmospheric Research, 1994.

Fichefet, T. and Maqueda, M. M.: Sensitivity of a global sea ice model to the treatment of ice thermodynamics and dynamics, J. Geophys. Res., 102, 12 609–12 646, 1997.

Gaspar, P., Gregorius, Y., and Lefevre, J.-M.: A simple eddy kinetic energy model for simulations of oceanic vertical mixing tests at Station Papa and Long-Term Upper Ocean Study Site, J. Geophys. Res., 95, 16 179–16 193, 1990.

Gent, P. R. and McWilliams, J. C.: Isopycnal mixing in ocean circulation models, J. Phys. Oceanogr., 20, 150–155, 1990.

Gent, P. R., Willebrand, J., McDougall, T. J., and McWilliams, J. C.: Parameterising eddy-induced tracer transports in ocean circulation models, J. Phys. Oceanogr., 25, 463–474, 1995.

GLOBALVIEW-CO_2: Cooperative Atmospheric Data Integration Project — Carbon Dioxide, CD-ROM, NOAA CMDL, Boulder,

Colorado [Also available on Internet via anonymous FTP to ftp.cmdl.noaa.gov, Path: ccg/co2/GLOBALVIEW], 2003.

Goose, H.: Modeling the large scale behaviour of the coupled ocean-sea ice system, Ph.D. thesis, Université Catholique de Louvain, Louvain-la-Neuve, Belgium, 1997.

Gordon, A. L.: Interocean exchange of thermocline water, J. Geophys. Res., 91, 5037–5046, 1986.

Griffies, S. M. and Hallberg, R. W.: Biharmonic friction with a Smagorinsky-like viscosity for use in large-scale eddy-permitting ocean models, Mon. Wea. Rev., Part 2, 128(8), 2935–2946, 2000.

Griffies, S. M., Boning, C., Bryan, F. O., Chassignet, E. P., Gerdes, R., Hasumi, H., Hirst, A., Treguier, A.-M., and Webb, D.: Developments in ocean climate modelling, Ocean Model., 2, 123–192, 2000.

Gruber, N., Sarmiento, J., and Stocker, T.: An improved method for detecting anthropogenic CO_2 in the oceans, Global Biogeochem. Cy., 10, 809–837, 1996.

Hallberg, R. W. and Gnanadesikan, A.: An exploration of the role of transient eddies in determining the transport of a zonally reentrant current, J. Phys. Oceanogr., 31, 3312–3330, 2001.

Hill, H., Hill, C., Follows, M., and Dutkiewicz, S.: Is there a computational advantage to offline tracer modeling at very high resolution?, Geophys. Res. Abstr., 6, EGU04-A-06348, 2004.

Hirst, A. and McDougall, T. J.: Deep-water properties and surface buoyancy flux as simulated by a z-coordinate model including eddy-induced advection, J. Phys. Oceanogr., 26, 1320–1343, 1996.

Holland, W. R.: The role of mesoscale eddies in the general circulation of the ocean: Numerical experiments using a wind-driven quasigeostrophic model, J. Phys. Oceanogr., 8, 363–392, 1978.

Holland, W. R. and Lin, L. B.: On the origin of mesoscale eddies and their contribution to the general circulation of the ocean. I. A preliminary numerical experiment, J. Phys. Oceanogr., 5, 642–657, 1975a.

Holland, W. R. and Lin, L. B.: On the origin of mesoscale eddies and their contribution to the general circulation of the ocean. II. A parameter study, J. Phys. Oceanogr., 5, 658–669, 1975b.

Holton, J.: An advective model for two-dimensional transport of stratospheric trace species, J. Geophys. Res., 86, 11 989–11 994, 1981.

Ito, T., Marshall, J., and Follows, M.: What controls the uptake of transient tracers in the Southern Ocean?, Global Biogeochem. Cy., 18, GB2021, doi:10.1029/2003GB002103, 2004.

Jackett, D. R. and McDougall, T. J.: Minimal adjustment of hydrographic profiles to achieve static stability, J. Atmos. Oceanic Technol., 12, 381–389, 1995.

Jakobsson, M., Cherkis, N., Woodward, J., Coakley, B., and Macnab, R.: A new grid of Arctic bathymetry: A significant resource for scientists and mapmakers, EOS Trans AGU, 81, 9, p. 89, 93, 96, 2000.

Joos, F., Orr, J. C., and Siegenthaler, U.: Ocean carbon transport in a box-diffusion versus a general circulation model, J. Geophys. Res., 102, 12 367–12 388, 1997.

Kalnay, E., Kanamitsu, M., Kistler, R., Collins, W., Deaven, D., Gandin, L., Iredell, M., Saha, S., White, G., Woollen, J., Zhu, Y., Chelliah, M., Ebisuzaki, W., Higgins, W., Janowiak, J., Mo, K. C., Ropelewski, C., Wang, J., Leetma, A., Reynolds, R., Jenne, R., and Joseph, D.: The NCEP/NCAR 40-year reanalysis project, B. Am. Meteorol. Soc., 77, 437–471, 1996.

Karsten, R. H. and Marshall, J.: Constructing the residual circulation of the ACC from observations, J. Phys. Oceanogr., 32, 3315–3327, 2002.

Key, R. M., Lee, C. L. S. K., Wanninkhof, R., Bullister, J., Feely, R. A., Millero, F. J., Mordy, C., and Peng, T.-H.: A Global Ocean Carbon Climatology: Results from Global Data Analysis Project (GLODAP, Global Biogeochem. Cy., 18, GB4031, doi:10.1029/2004GB002247, 2004.

Levitus, S., Boyer, T., Conkright, M., O'Brian, T., Antonov, J., Stephens, C., Stathopolos, L., Johnson, D., and Gelfeld, R.: World Ocean Database 1998, Tech. rep., NOAA Atlas NESDIS 18, 1998.

Lévy, M., Klein, P., and Treguier, A.: Impacts of sub-mesoscale dynamics on phytoplankton production and subduction, J. Mar. Res., 59, 535–565, 2001.

Lythe, M. and Vaughan, D.: BEDMAP: a new ice thickness and subglacial topographic model of Antarctica, J. Geophys. Res., 106(B6), 11 335–11 351, 2001.

Madec, G. and Imbard, M.: A global ocean mesh to overcome the North Pole singularity, Clim. Dynam., 12, 381–388, 1996.

Madec, G., Delecluse, P., Imbard, M., and Lévy, C.: OPA version 8.0, Ocean General Circulation Model, Reference Manual., Note of the IPSL Modelling Pole 11, IPSL, 1998.

Marshall, J. and Radko, T.: Residual-mean solutions for the Antarctic Circumpolar Current and its associated overturning circulation, J. Phys. Oceanogr., 33, 2341–2354, 2003.

Marshall, J., Jones, H., Karsten, R., and Wardle, R.: Can Eddies Set Ocean Stratification?, J. Phys. Oceanogr., 32, 26–38, 2002.

Marshall, J. C. and Nurser, A. J. G.: Fluid dynamics of the oceanic thermocline ventilation, J. Phys. Oceanogr., 22, 583–595, 1992.

Marti, O., Madec, G., and Delecluse, P.: Comment on "Net diffusivity in ocean general circulation models with non uniform grids" by F. L. Yin and I. Y. Fung, J. Geophys. Res., 97, 12 763–12 766, 1992.

Matear, R. J.: Effects of numerical advection schemes and eddy parameterisations on ocean ventilation and oceanic anthropogenic CO2 uptake, Ocean Model., 3, 217–248, 2001.

Matsumoto, K. and Gruber, N.: How accurate is the estimation of anthropogenic carbon in the ocean? An evaluation of the ΔC^* method, Global Biogeochem. Cy., 19, GB3014, doi:10.1029/2004GB002397, 2005.

Matsumoto, K., Sarmiento, J. L., Key, R. M., Aumont, O., Bullister, J. L., Caldeira, K., Campin, J.-M., Doney, S. C., Drange, H., Dutay, J.-C., Follows, M., Gao, Y., Gnanadesikan, A., Gruber, N., Ishida, A., Joos, F., Lindsay, K., Maier-Reimer, E., Marshall, J. C., Matear, R. J., Monfray, P., Mouchet, A., Najjar, R., Plattner, G.-K., Schlitzer, R., Slater, R., Swathi, P. S., Totterdell, I. J., Weirig, M.-F., Yamanaka, Y., Yool, A., and Orr, J. C.: Evaluation of ocean carbon cycle models with data-based metrics, Geophys. Res. Lett., 31, L07303, doi:10.1029/2003GL018970, 2004.

McDougall, T. J.: Neutral surfaces, J. Phys. Oceanogr., 17, 1950–1964, 1987.

McIntosh, P. C. and McDougall, T. J.: Isopycnal averaging and the residual mean circulation, J. Phys. Oceanogr., 26, 1655–1660, 1996.

Orr, J. C., Monfray, P., Maier-Reimer, E., Mikolajewicz, U., Palmer, J., Taylor, N. K., Toggweiler, J. R., Sarmiento, J. L., Quéré, C. L., Gruber, N., Sabine, C. L., Key, R. M., and Boutin, J.: Estimates

of anthropogenic carbon uptake from four three-dimensional global ocean models, Global Biogeochem. Cy., 15, 43–60, 2001.

Price, J. F.: Ocean Circulation and Climate: Observing and Modelling the Global Ocean, Chap. Subduction, Academic Press, 357–371, 2001.

Rintoul, S. R.: South Atlantic interbasin exchange, J. Geophys. Res., 96, 2675–2692, 1991.

Robbins, P. E., Price, J. F., Owens, W., and Jenkins, W.: On the importance of lateral diffusion for the ventilation of the lower thermocline in the Subtropical North Atlantic, J. Phys. Oceanogr., 30, 67–89, 2000.

Sabine, C. L., Feely, R. A., Gruber, N., Key, R. M., Lee, K., Bullister, J. L., Wanninkhof, R., Wong, C. S., Wallace, D. W. R., Tilbrook, B., Millero, F. J., Peng, T.-H., Kozyr, A., Ono, T., and Rios, A.: The ocean sink for anthropogenic CO_2, Science, 305, 367–370, 2004.

Sarmiento, J. L. and Gruber, N.: Ocean Biogeochemical Dynamics, Princeton University Press, 2006.

Sarmiento, J. L., Orr, J. C., and Siegenthaler, U.: A perturbation simulation of CO_2 uptake in an ocean general circulation model, J. Geophys. Res., 97, 3621–3645, 1992.

Sarmiento, J. L., Le Quéré, C., and Pacala, S. W.: Limiting future atmospheric carbon dioxide, Global Biogeochem. Cy., 9, 121–137, 1995.

Sasai, Y., Ishida, A., Yamanaka, Y., and Sasaki, H.: Chlorofluorocarbons in a global ocean eddy-resolving OGCM: Pathway and formation of Antarctic Bottom Water, Geophys. Res. Lett., 31, L12305, doi:10.1029/2004GL019895, 2004.

Sen Gupta, A. and England, M.: Evaluation of interior circulation in a high resolution global ocean model, Part I: Deep and Bottom Waters, J. Phys. Oceanogr., 34, 2592–2614, 2004.

Siegenthaler, U. and Joos, F.: Use of a simple model for studying oceanic tracer distributions and the global carbon cycle, Tellus, 44B, 186–207, 1992.

Smith, W. H. F. and Sandwell, D. T.: Global seafloor topography from satellite altimetry and ship depth soundings, Science, 277, 1957–1962, 1997.

Smolarkiewicz, K. P.: The multidimensional Crowley advection scheme, Mon. Wea. Rev., 110, 1968–1983, 1982.

Smolarkiewicz, K. P.: A simple positive advection scheme with small implicit diffusion, Mon. Wea. Rev., 111, 479–486, 1983.

Smolarkiewicz, K. P. and Clark, T. L.: The multidimensional positive definite advection transport algorithm: further development and applications, J. Comp. Phys., 67, 396–438, 1986.

Steele, M., Morley, R., and Ermold, W.: PHC: A global ocean hydrography with a high quality Arctic Ocean, J. Climate, 14, 2079–2087, 2001.

Thompson, S. R., Stevens, D. P., and Döös, K.: The importance of interocean exchange south of Africa in a numerical model, J. Geophys. Res., 102, 3303–3315, 1997.

Toggweiler, J. R., Dixon, K., and Bryan, K.: Simulations of radiocarbon in a coarse resolution world ocean model 1. Steady state prebomb distributions, J. Geophys. Res., 94, 8217–8242, 1989a.

Toggweiler, J. R., Dixon, K., and Bryan, K.: Simulations of radiocarbon in a coarse resolution world ocean model 2. Distributions of bomb-produced carbon 14, J. Geophys. Res., 94, 8243–8264, 1989b.

Trenberth, K. E., Olson, J. G., and Large, W. G.: A global ocean wind stress climatology based on ECMWF analyses, Report NCAR/TN-338 +STR, National Center for Atmos. Res., Boulder, Colorado, 93 pp., 1989.

Vallis, G. K.: Thermocline theories and WOCE: A mutual challenge, International WOCE Newsletter, 39, WOCE International Project Office, Southampton, UK, 3–5, 2000.

Walker, S., Weiss, R., and Salameh, P.: Reconstructed histories of the annual mean atmospheric mole fractions for halocarbons CFC-11, CFC-12, CFC-113, and carbon tetrachloride., J. Geophys. Res., 105, 14 285–14 296, 2000.

Wallace, D. and Lazier, J.: Anthropogenic chlorofluoromethanes in newly formed Labrador Sea water, Nature, 332, 6163, 1988.

Wanninkhof, R.: Relationship between wind speed and gas exchange over the ocean, J. Geophys. Res., 97, 7373–7382, 1992.

Warner, M. and Weiss, R.: Chlorofluoromethanes in South Atlantic Antarctic Intermediate Water, Deep-Sea Res., 39, 2053–2075, 1992.

Watson, A. J. and Orr, J. C.: Carbon dioxide fluxes in the global ocean, in: Ocean Biogeochemistry: the Role of the Ocean Carbon Cycle in Global Change (a JGOFS Synthesis), Chap. 5, edited by: Fasham, M., Field, J., Platt, T., and Zeitzschel, B., Springer, Berlin, 123–141, 2003.

Waugh, D. W., Hall, T. M., and Haine, T. W. N.: Relationships among tracer ages, J. Geophys. Res., 108(C5), 3138, doi:10.1029/2002JC001325, 2003.

Willey, D. A., Fine, R. A., Sonnerup, R. E., Bullister, J. L., Smethie Jr., W. M., and Warner, M. J.: Global oceanic chlorofluorocarbon inventory, Geophys. Res. Lett., 31, L01303, doi:10.1029/2003GL018816, 2004.

Xie, P. and Arkin, P. A.: Analyses of global monthly precipitation using gauge observations, satellite estimates and numerical model predictions, J. Climate, 9, 840–858, 1996.